# Inter-crosslinked Spirocyclic Mixed Matrix Membranes Exhibiting Enhanced Gas Permeability, Selectivity, and Plasticization Resistance

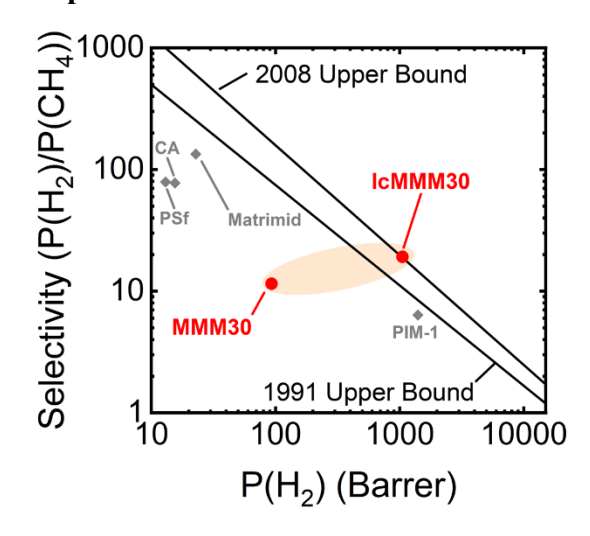
Lucas C. Condes, Adriana E. Landry, Matthew T. Webb, William J. Box, Aditi Gali, and Michele Galizia\*

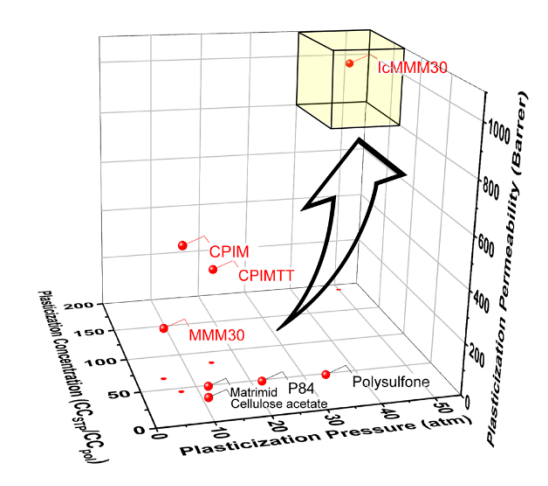
School of Sustainable Chemical, Biological and Materials Engineering, University of Oklahoma, 100 E. Boyd Street, Norman 73019, OK, USA

Revised Manuscript, June 25th, 2024

\* Corresponding Author: Prof. Michele Galizia, mgalizia@ou.edu

# **Graphical Abstract**





# Highlights

- Highly selective and stable inter-crosslinked MMMs were synthesized
- Polymer-filler thermal crosslinking leads to superior plasticization stability
- Thermal crosslinking was achieved at temperatures as low as 200°C
- Inter-crosslinked MMMs show defect-free behavior up to 30 wt. % PPN loading
- The roles of physical and chemical polymer-filler interactions were elucidated

#### Abstract

Poor interfacial compatibility is the most common issue inhibiting performance enhancement in mixed matrix membranes (MMM) for gas and liquid separations. To address this issue, we fabricated highly selective and permeable inter-crosslinked mixed matrix membranes (IcMMMs) based on carboxylic-acid functionalized polymer of intrinsic microporosity-1 (CPIM) containing up to 30 wt. % triptycene-isatin polymer porous network (PPN) particles. Polymer-filler intercrosslinking is accomplished via thermal decarboxylation at 200°C, which is the lowest temperature this reaction has been found to occur in the literature. This low temperature circumvents potential issues with degradation of porous supports or gutter layer materials, and thus enables these materials to be integrated into traditional membrane processes. The resulting IcMMMs exhibit gel fractions above 90%. Beyond IcMMMs, membranes based on neat CPIM, thermally crosslinked CPIM, as well as non-crosslinked CPIM-PPN mixed matrix membranes were fabricated to elucidate the individual and synergistic effects of filler inclusion and thermal treatment. In addition to showing upper bound permeability-selectivity performance, IcMMMs also exhibit an almost unprecedented stability against plasticization upon extended exposure to CO<sub>2</sub> up to 50 atm or above. This study shows that crosslinking across the polymer-filler interface is the key feature to achieve simultaneous enhancement in permeability, selectivity, and stability. To elucidate the molecular mechanism of these enhancements in the IcMMMs with respect to the baseline materials, permeability was broken into its sorption and diffusion contributions and an energetic analysis of sorption was performed. The low cost of PPNs coupled with the mild crosslinking temperature make this approach highly scalable, resulting in materials exhibiting high rigidity and structural stability with the potential to excel in aggressive separations, such as organic solvent separations or high-CO<sub>2</sub> content, high-pressure natural gas sweetening.

### **Keywords**

mixed matrix membranes; thermal crosslinking; plasticization resistance; carboxylated PIM; porous polymer networks

# 1. Introduction

Chemical separations account for a significant fraction of global energy consumption, which is estimated to be 8 GJ per person on the hearth every year [1]. Although membrane separations hold promise as energy efficient and sustainable alternatives to thermal-based separations, their large-scale implementation has been hindered by long-standing challenges, such as poor selectivity and stability. These challenges are especially difficult to solve within the context of the chemically and thermally harsh operating conditions in applications such as sour gas processing, carbon capture, hydrogen production, and organic solvent separation [1–3].

A trade-off relationship between permeability and selectivity exists in polymer membranes, wherein attempts to enhance permeability are typically accompanied by a loss in selectivity, and vice-versa [4,5]. While strides in enhancing permeability while maintaining modest selectivity have continually been made by synthesizing extremely rigid polymer architectures, improving selectivity without significantly compromising permeability has proven to be a challenge [3,6,7]. As recommended by the US National Academies in 2019 [8], enhancing permeability and selectivity, while important, is not sufficient. The long-term stability of membrane permeability and selectivity remains a mostly unsolved challenge. Many existing state-of-the-art polymer membranes based on linear glassy polymers, despite exhibiting adequate separation performance in the short term, suffer from poor long-term stability due to plasticization and physical aging [9,10]. A generally accepted idea is that the suppression of chain rotation *via* the use of monomers exhibiting fused rings, such as those found in polybenzimidazoles (PBIs), might help fix this issue. However, these polymers still exhibit a marked aging and plasticization propensity [11,12]. Spirocyclic polymers, such as polymers of intrinsic microporosity (PIMs), are another example of functional materials designed to exhibit high permeability and rigidity. PIMs typically consist of a combination of rigid kinked moieties, such as spiro centers, which generate internal microporosity, and fused rings, which hamper chain rotation. Since their discovery, a plethora of functionalization approaches have been devised to engineer their properties by direct substitution of the nitrile groups. A large variety of substitutions have been proposed, such as amidoximes [13,14], carboxylic acids [15,16], amines [17–19], amides [20,21], thioamides [22], and tetrazoles [23]. Despite their positive effects on permeability and selectivity in the short time frame, these approaches alone are not sufficient to fix long-term stability issues [10,14,15,17,18].

Although increasing monomer rigidity inhibits atomic-scale fluctuations, polymer chain mobility must be halted to guarantee a stable performance in chemically and thermally harsh environments [10]. The core challenge to be addressed is to synthesize materials exhibiting, even in harsh environments, a permanent structure at multiple length scales, while maintaining a free volume architecture capable of offering adequate size sieving ability. Solving this challenge requires simultaneous freezing of local atomic fluctuations to preserve permeability and selectivity (i.e., rigid/kinked monomers) [24], as well as reduction of the chain mobility responsible for plasticization and physical aging. Thus, a *combination* of both rigid molecular architectures and chain immobilization techniques could be a favorable strategy to produce membranes meeting the expected needs.

Fabricating immobilized molecular architectures presents a distinct challenge when considering that polymers should be solvent-soluble and go through a vitrification process during fabrication as a thin film. This process inherently produces non-equilibrium (i.e., glassy) materials with some degree of chain mobility. Given this conflict between the nature of membrane processing and the need for stable materials, fabrication of highly stable membranes often requires post-modification chemical treatments, thermal treatments, or the incorporation of additives [3,25–27].

Crosslinking is an effective approach to immobilize polymer chains, leading to membranes exhibiting enhanced plasticization resistance [28–34]. Polyimides (PIs) exhibiting carboxylic groups were crosslinked using various diols or multivalent metal ion coordination to the carboxylate form. This result was generally successful and resulted in films exhibiting adequate plasticization resistance upon exposure to CO<sub>2</sub> up to 30-40 atm [28–30]. In 2008, Kratochvil and Koros used thermal decarboxylation at 389°C to crosslink diamino benzoic acid (DABA) containing PIs, followed by rapid quenching [31]. This decarboxylation approach was more effective than the diol crosslinking, as it produced membranes exhibiting plasticization resistance up to 45 atm, with a CO<sub>2</sub> permeability at plasticization of 450 Barrer. Of equal importance, these membranes resisted hydrolysis and did not require external crosslinking agents. The crosslinking temperature, however, was above the polymer's T<sub>g</sub>, which may be problematic if the polymer experiences degradation below its glass transition. Decarboxylation crosslinking has been successfully extended and combined into hybrid approaches to modify polyimides [32,35–37], PIMs [34], Tröger's base polymers [38], and thermally rearranged polymers [39]. All these approaches, however, rely on crosslinking temperatures above 300 °C, which makes the processing

and scale-up of these membranes difficult, as conventional gutter layers or porous support materials do not withstand such high temperatures. Additionally, many of these crosslinked films still exhibit performance instabilities under harsh conditions, especially when fabricated as thin films [32]. In this study, we propose a fabrication approach capable of producing fully crosslinked spirocyclic polymers at temperatures as low as 200°C, where most of porous support will not experience any degradation issues.

Another approach to enhance selectivity and stability relies on the incorporation of porous materials in polymers to fabricate mixed matrix membranes (MMM). While zeolites were initially considered, researchers have turned to designing metal organic frameworks (MOFs) and other hybrid porous materials due to their better compatibility with polymers. Overall, the MMM approach offers the well-defined and permanent structure of the incorporated particles, but it also introduces the need to engineer polymer-filler interactions, find optimal filler loadings, and design new fabrication routes. Solving the problem of poor polymer-filler compatibility, which compromises selectivity due to the formation of defects at filler-polymer interfaces, has been of particular focus [40,41]. Recently, the discovery of new synthetic routes made it possible to fabricate fully organic porous fillers, such as porous organic cages (POCs), porous aromatic frameworks (PAFs), and porous polymer networks (PPNs) [42,43]. These materials exhibit some key features, such as i) lack of inorganic components, ii) tunable porosity and microporosity, and iii) capability of being functionalized. These features tend to eliminate the structural defects typically observed in conventional MMMs by promoting intimate polymer-filler blending. In some instances, these organic additives establish physical and chemical interactions with the polymer, such that the blend resembles a single phase rather than a heterogeneous medium. For this reason, these material systems have been called molecularly mixed composite membranes (MMCMs). Lively et al. fabricated MMCMs for organic solvent separations exhibiting molecular weight cutoff below 236 g/mol in methanol, ethanol, and toluene in organic solvent nanofiltration (OSN) tests [44]. Noteworthy, this approach may also benefit membrane's long-term stability. Indeed, as shown by Noble et al., incorporation of PAFs significantly reduces the aging propensity of high free volume microporous glassy polymers, such as PTMSP and PIM-1 [45,46].

In this study, we combine the crosslinking and mixed matrix membrane approaches to design polymer membranes exhibiting simultaneously high selectivity, high stability and superb plasticization resistance. We demonstrate that PPNs synthesized from isatin and triptycene can be blended with carboxylic-acid functionalized PIM-1 (CPIM) to form defect-free MMMs at loadings as high as 30 wt. %. Thermally induced decarboxylation crosslinking is then utilized to crosslink not only CPIM to itself, but the CPIM to the PPN. These composite membranes, wherein the filler and continuous phase are chemically bonded, are thus specified as *inter-crosslinked mixed matrix membranes* (IcMMMs). Notably, crosslinking is accomplished at 200°C, which is the lowest temperature this reaction has been found to occur in the literature. This low temperature circumvents potential issues with degradation of porous supports or gutter layer materials, thus facilitating the scale up and integration of these materials into membrane processes. The low cost of PPNs compared to other fillers, such as PAFs (50 vs 500 \$/g), improves the scalability of the proposed approach. The resulting IcMMMs exhibit upper bound permeability-selectivity performance for several gas pairs and an impressive CO<sub>2</sub> plasticization resistance up to at least 50 atm for extended exposure times, which places these membranes among the most stable ever reported. Finally, fundamental structure-property correlations are presented to explain the molecular origin of the observed behaviors.

# 2. Theoretical Background

Pure gas permeability (P) in dense membranes is described by the solution-diffusion model:

$$P = \overline{D} \times S \tag{Eq. 1}$$

where  $\overline{D}$  is the concentration-averaged diffusion coefficient and S is the solubility coefficient given by the fugacity-normalized penetrant concentration in the polymer phase (i.e., C), so that S = C/f. Based on the solution-diffusion model, the ideal permeability-selectivity of gases A and B,  $\alpha_{A/B}$ , is defined as follows:

$$\alpha_{A/B} = \frac{P_A}{P_B} = \frac{D_A}{D_B} \times \frac{S_A}{S_B}$$
 (Eq. 2)

where  $(\frac{D_A}{D_B})$  and  $(\frac{S_A}{S_B})$  are the diffusion-selectivity (i.e. size-sieving ability) and the solubility-selectivity, respectively.

The dual mode sorption/transport model describes small molecule sorption and transport in glassy polymers by envisioning the polymer phase as a heterogeneous medium (i.e, Henry's and Langmuir's contributions):

$$C = k_D f + \frac{C'_H b f}{1 + b f}$$
 (Eq. 3)

where C is the penetrant concentration in the polymer, f is the fugacity in the external gas phase,  $k_D$  is the Henry's solubility coefficient,  $C'_H$  is the Langmuir sorption capacity, and b is the Langmuir affinity parameter [15,47].

Fundamental insights into the penetrant-polymer and penetrant-penetrant interactions responsible for the membrane transport behavior can be gained by examining the energetics of penetrant sorption in the membrane material. Isosteric heats are the enthalpy of sorption at constant penetrant concentration in the polymer phase. The enthalpy of sorption is the difference in enthalpy between a penetrant in the bulk gas phase and the same penetrant when condensed in the polymer phase. The isosteric heat is related to energetic changes due to condensation of the penetrant, interaction of the penetrant with the polymer, and interaction of the penetrant with other penetrants already in the polymer phase [48]. In this work, isosteric heats are used to base the membrane plasticization propensity on a rational thermodynamic basis. Isosteric heats of sorption were determined by collecting gas sorption isotherms at multiple temperatures, as follows [48]:

$$\left(\frac{d(\ln p)}{d(\frac{1}{T})}\right)_{C} = \frac{\Delta H_{S}}{R}$$
 (Eq. 4)

where p is the pressure at which the penetrant concentration C is achieved, T is the temperature, R is the gas constant, and  $\Delta H_S$  is the isosteric heat.

Besides equilibrium gas uptake, the dual-mode model has also been adapted to describe the diffusion of gases in each of the two modes, assuming the existence of a distinct contribution of penetrant mobility from each sorbed mode in the polymer rather than a single representative diffusion coefficient [47,49]. Therefore, according to the partial immobilization model, the gas permeability P can be expressed as follows:

$$P = k_D D_D + \frac{c_H' b D_H}{1+b f}$$
 (Eq. 5)

where  $D_D$  and  $D_H$  are the Henry mode and Langmuir mode diffusion coefficients, respectively. The ratio of the two diffusion coefficients is given as the parameter F, where  $F = D_H/D_D$ . A value of F = 0 represents the 'total immobilization' case wherein gases sorbed in Langmuir sites do not contribute to the measured diffusivity, whereas a value of F = 1 corresponds to 'no immobilization' wherein the diffusion behavior of gases does not depend on which sorbed mode the gas occupies.

# 3. Experimental Methods

- 3.1. Materials. Details about the chemicals used and their purification routes are provided in the Supporting Information (SI), Section S1.
- 3.2. Synthesis of PIM-1. PIM-1, the precursor material for carboxylated PIM-1 (CPIM), was synthesized as shown in Figure 1A, via high-temperature polycondensation. Details are provided in the SI, Section S2.

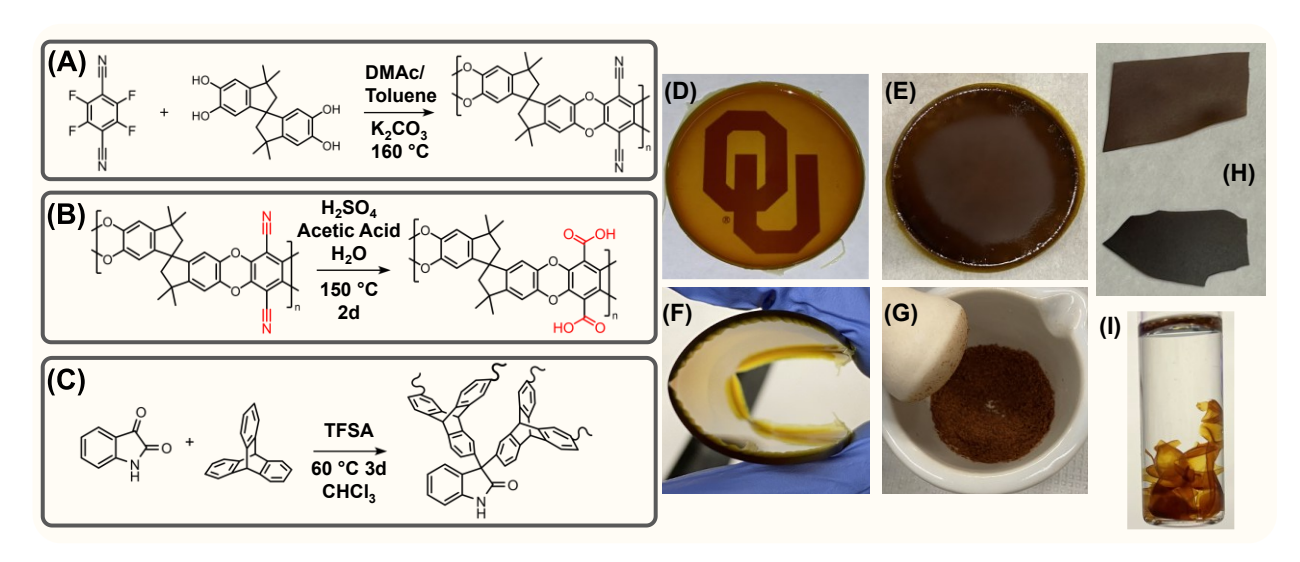


**Figure. 1.** Synthetic routes to (A) PIM-1, (B) CPIM, and (C) triptycene isatin PPN. (D and F) defect-free CPIM membranes, (E) a defect-free MMM30 membrane, (G) the synthesized triptycene isatin powder, (H) color comparison of a MMM30 membrane before (top) and after (bottom) thermal treatment, and (I) demonstration of CPIMTT's insolubility after soaking in THF for 24h.

3.3 Acid Hydrolysis of PIM-1. Carboxylated PIM-1, denoted herein as CPIM, was prepared via the acid hydrolysis method with minor modifications (cf., Figure 1B) [15]. Specifically, 0.8 g of PIM-1 was combined with 48 mL of deionized (DI) water, 16 mL of glacial acetic acid, and 48 mL of sulfuric acid in a 250 mL single neck round-bottom flask equipped with a water-cooled condenser and magnetic stir bar. The reaction was heated by submersion of the flask in an oil bath at 150°C under stirring at 200 rpm. After 48h, the reaction mixture was decanted into 500 mL of water. The resulting solution was filtered to recover a brown-colored product. To retain the protonated form of the acid groups, the product was refluxed in 200 mL of DI water with 3-4 drops of sulfuric acid

for 24h. Finally, the final product was recovered by filtration and dried in a vacuum oven at 110°C overnight. The degree of carboxylation, determined via elemental analysis, was about 90% (cf. Table 1).

3.4 Synthesis of Triptycene-Isatin Porous Polymer Network. Porous polymer networks (PPN) were synthesized in-house via the hydroxyalkylation reaction between triptycene and isatin (cf., Figure 1C). Details regarding the synthesis procedure are provided in the SI, Section S3, along with some relevant PPNs properties. The rationale for selecting triptycene-isatin PPN to be mixed with CPIM is that carboxy moieties in the CPIM backbone are expected to produce, upon thermal treatment, radical crosslinking with the triptycene moieties in the PPN to favor the formation of IcMMMs. Also, triptycene units provide their unique internal free volume, referred to as configurational free volume [50–52], which exhibits extremely uniform distribution, offering high selectivity as well as long-term stability [42]. Finally, isatin, which is an activated ketone exhibiting high reactivity in the hydroxyalkylation reaction, is cheap, readily available, and contains amide groups that can favorably interact with gases such as CO<sub>2</sub>.

3.5. Membrane Fabrication. In this study, four kinds of membranes were fabricated: neat CPIM, thermally treated (i.e., thermally crosslinked) CPIM, mixed matrix membranes comprising CPIM and 30 wt. % PPN (MMM), and thermally treated membranes of CPIM and 30 wt. % PPN (i.e., IcMMMs). A loading of 30 wt. % PPN is the previous highest successful loading achieved in the literature, and this loading was used throughout this study to serve as a benchmark for comparison [43]. All membranes were fabricated via solution casting. Details are reported in the SI, Section S4.

After fabrication, dense, self-standing (i.e., support-free) membranes, 140-180 µm thick, were thermally crosslinked by placing them in a glass petri dish in a room-temperature vacuum oven equipped with a cold trap, which was filled with liquid nitrogen. Vacuum was pulled for 30 minutes to remove gases and any residual moisture. Following this step, the oven was heated to 200 °C over the course of one hour. The samples were held at this temperature under vacuum for 24h, and then were allowed to slowly cool to room temperature. This procedure avoids any potential oxidation processes that could complicate the crosslinking process. Regarding sample

nomenclature, the uncrosslinked MMM containing 30 wt.% PPN will be denoted MMM30, and the thermally crosslinked IcMMM containing 30 wt. % PPN will be called IcMMM30 throughout the manuscript. Thermally crosslinked CPIM will be denoted CPIMTT. PPN-containing samples had a darker appearance, and the color darkened further upon thermal treatment, as shown in Figures 1D-H. As shown in Figure 1I, both thermally crosslinked membranes (i.e., CPIM-TT and IcMMM30) are insoluble in THF.

- 3.6. Structural Characterization. Details regarding the compositional (NMR, FTIR, elemental analysis), thermal (DSC, TGA-MS), and physical (BET, gel fraction) characterization are provided in the SI, Sections S5-12.
- 3.7 Sorption/Transport Measurements and Plasticization Study. Pure gas H<sub>2</sub>, CH<sub>4</sub>, and CO<sub>2</sub> permeability was measured at 35 °C and up to 30 atm using a constant volume, variable pressure apparatus. Details are provided in the SI, Section S13.

High pressure CO<sub>2</sub> permeability measurements were run, up to 50 atm at 35 °C, to assess membrane plasticization resistance. Membranes were first exposed to a low CO<sub>2</sub> pressure (0.2-0.5 atm), which was increased stepwise until a discernible minimum in permeability was observed. Permeability rise due to CO<sub>2</sub>-induced plasticization is a transient dynamic process dependent on polymer relaxation, and steady increases in permeability can be observed to occur for multiple days at constant CO<sub>2</sub> pressures [29,32,53]. Thus, a standard procedure was determined to equalize the membrane exposure time to each CO<sub>2</sub> pressure, wherein each CO<sub>2</sub> pressure was held for 24 hours, and the downstream side of the membrane was vacuumed out until measurement at the end of each 24 hours.

To gain fundamental insights into the transport mechanism via the dual-mode model, pure gas CO<sub>2</sub> and CH<sub>4</sub> sorption was measured at temperatures between 15-50°C and up to 40 atm, using the pressure decay method [54]. H<sub>2</sub> was excluded from sorption measurements, due to its extremely low condensability [55]. Details regarding the sorption measurements are provided in the SI, Section S14. Diffusion coefficients were determined from experimental sorption and permeation data, using the solution-diffusion model.

### 4. Results and Discussion

4.1 *Synthesis and Characterization of PIM-1, CPIM, and Triptycene-Isatin PPN.* Successful synthesis of PIM-1, CPIM, and the triptycene-isatin PPN was confirmed by ATR-FTIR, 1H NMR, and <sup>13</sup>C NMR spectroscopy. Chemical structures of PIM-1 and CPIM are shown in Figure 2A-B, where they are labelled with the corresponding NMR proton or carbon assignments.

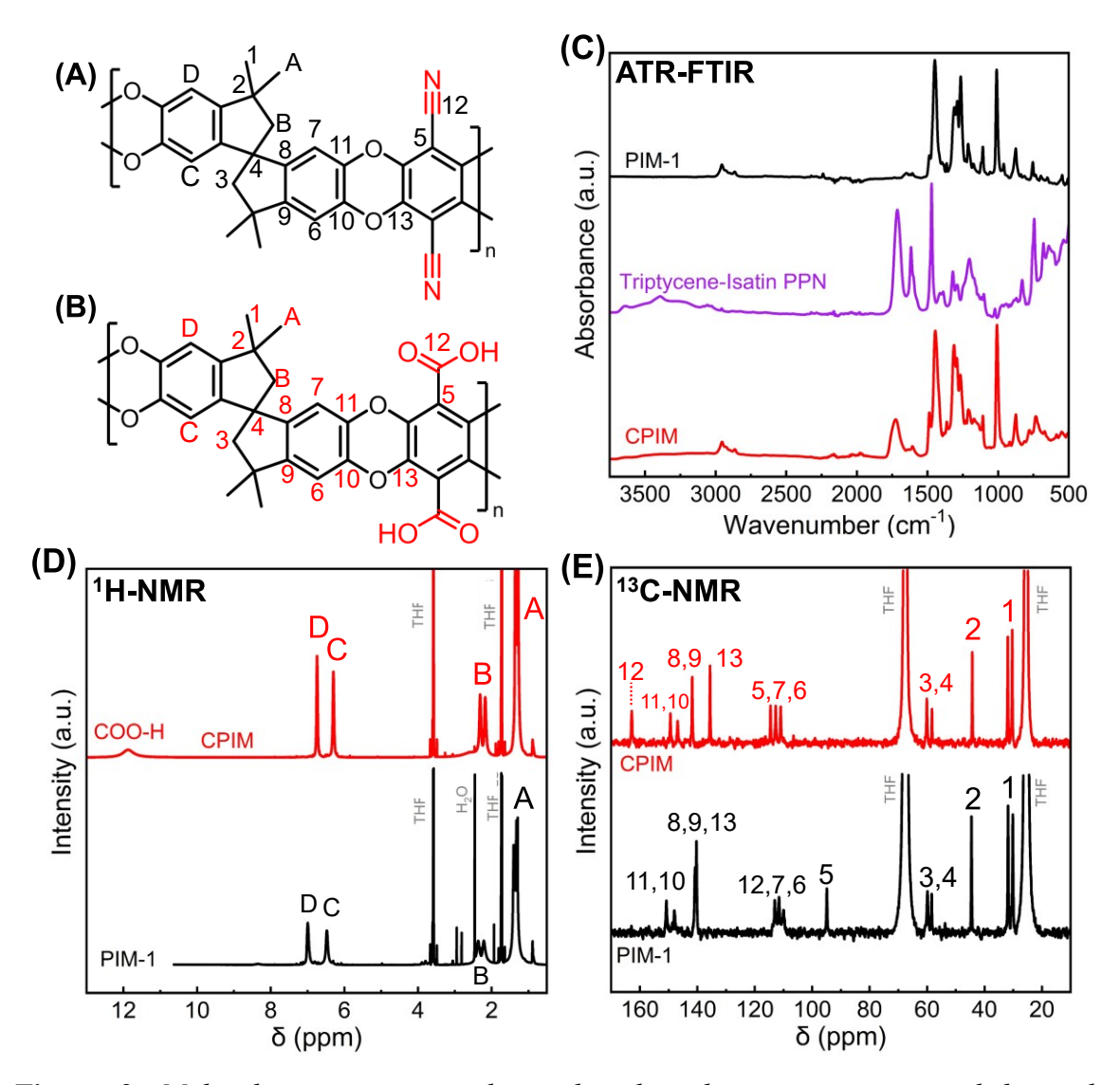


**Figure 2.** Molecular structures with numbered carbon assignments and lettered proton assignments for (A) PIM-1 and (B) CPIM. (C) ATR-FTIR, (D) <sup>1</sup>H NMR, and (E) <sup>13</sup>C NMR spectra of the synthesized materials are shown.

In Figure 2C, the ATR-FTIR spectra of the synthesized materials are shown. Both PIM-1 and CPIM exhibit the characteristic IR absorption bands, namely, the C=C aromatic stretching at 1600 cm<sup>-1</sup> [56,57], the dibenzodioxane C-O-C stretch at 1010 cm<sup>-1</sup> [58,59], as well as the methyl, methylene bridge, and aromatic stretching and bending peaks at 2840-3000 cm<sup>-1</sup> and 1360-1490 cm<sup>-1</sup>, respectively [57,60,61]. PIM-1 exhibits the characteristic nitrile C≡N stretch at 2238 cm<sup>-1</sup>, which disappears in CPIM. The latter, instead, exhibits new peaks appearing as a broad -OH stretch near 3500 cm<sup>-1</sup>, as well as a carbonyl stretch at 1720 cm<sup>-1</sup> corresponding to the carboxylic acid -COOH group [15]. The triptycene-isatin PPN exhibits the typical C=O stretch at 1708 cm<sup>-1</sup>, N-H bend at 1469 cm<sup>-1</sup>, and C-N stretch at 1320 cm<sup>-1</sup> characteristic of the lactam moiety [42]. Details about the PPN BET area and thermal stability are provided in the Supporting Information, sections S9 and S15, respectively.

<sup>1</sup>H NMR spectra for CPIM and PIM-1 are shown in Figure 2D. The peaks for the PIM-1 backbone (labeled A, B, C, D) are invariant between the PIM-1 and CPIM spectra and correspond to the expected structures for these materials [15,62]. Successful carboxylation of PIM-1 is confirmed by the appearance of the acidic proton signal in the <sup>1</sup>H NMR spectrum for CPIM at 11.9 ppm. In the <sup>13</sup>C spectra for PIM-1 and CPIM (cf., Figure 2E), the corresponding backbone peaks are preserved as in the case of the <sup>1</sup>H NMR spectra, and the almost complete shifting/disappearance of the signal at 95 ppm (i.e. carbon 5) and appearance of a signal at 162.9 ppm characteristic of the -COOH group in the <sup>13</sup>C spectrum of CPIM further confirm a successful carboxylation reaction [15,62,63].

To determine the degree of hydrolysis of CPIM (i.e., number of nitriles in PIM-1 converted to carboxylic acid groups in CPIM), combustion elemental analysis was performed. Elemental analysis was chosen since direct quantification by integration of <sup>1</sup>H NMR peaks is difficult to achieve due to exchange of the acidic protons with water [15,64]. Moreover, estimates from mass losses during decarboxylation would underestimate the degree of decarboxylation [15,62] since this process is self-catalyzed by nearby acid groups, therefore complete decarboxylation is not generally observed to occur in a single isolated mass loss during TGA analysis [31,65]. As shown in Table 1, the experimental *N/C* mass ratio in neat PIM-1 matches theoretical predictions, and the calculated degree of hydrolysis of the synthesized CPIM is 92.0%. This conversion is in agreement with literature data [15]. Since a dilute sulfuric acid solution is applied in the last processing step, a certain amount of sulfur is expected to be retained in the final CPIM product. Consistently, a

slight increase in the sulfur content between PIM-1 and CPIM (~0.3 wt. %) is apparent. Some implications of this residual acid content will be discussed in Section 4.2.

**Table 1**: Elemental analysis, in terms of atomic weight percents, of the synthesized PIM-1 and CPIM. The degree of hydrolysis is the percentage of nitrile groups in PIM-1 that have been converted into carboxylic acids. Sulfur (S) was tested to determine whether residual sulfuric acid was retained in the final product.

sample	data source	% C	% N	% S	N/C	degree of hydrolysis (%)
PIM-1	Experimental	72.97	5.83	0.21	0.08	0
	Theory	75.64	6.08	0	0.080	0
CPIM	Experimental	63.7	0.41	0.504	0.00637	92.0
	Theory	69.9	0	0	0	100

4.2 *Membrane Formation and Thermal Crosslinking*. Decarboxylation crosslinking has been successfully achieved in various acid-containing polyimides and microporous polymers, including CPIM, but usually at temperatures in excess of 300°C [31,33,35,38]. Significant losses in crosslinking efficiency and plasticization resistance have been reported as crosslinking temperature is decreased from 425°C to as low as 300°C for both polyimides and microporous PIMs [33,35,38]. Given that the temperature used in this study (200°C) for the decarboxylation crosslinking reaction is relatively low, gel fraction analysis, FTIR, 13C CP/MAS NMR, and TGA-MS were used to confirm that crosslinking successfully occurred, as well as to quantify the extent of crosslinking.

The gel fraction characterizes the amount of insoluble material of a crosslinked gel. By using THF, a good solvent for CPIM, soluble material was leached out of crosslinked membranes (i.e., CPIMTT and IcMMM30), and the fraction of remaining mass gives an estimate of the crosslinking efficiency. Du et al. previously reported, for CPIMs crosslinked at  $375^{\circ}$ C for 40 minutes, gel fractions of 85-92% with degrees of hydrolysis of 85-100% [34]. For the CPIM reported herein, with a 92% degree of hydrolysis, the gel fraction of the resulting crosslinked (i.e., thermally treated) membrane, CPIMTT, is  $90 \pm 1\%$ . The thermally crosslinked IcMMM30 exhibits a gel

fraction of 94.1  $\pm$  0.7%. Remarkably, these results confirm that crosslinking efficiency is not sacrificed by the lower crosslinking temperature. To the best of our knowledge, this is the first time that thermal crosslinking of PIM derivatives has been achieved at temperatures as low as 200°C [34,66,67].

One possibility is that crosslinking occurs by formation of anhydrides, rather than by formation of covalent C-C bonds. However, the presence of anhydrides as primary crosslinking products was ruled out by hydrolysis testing, wherein samples of CPIMTT were boiled in water for 10 days, after which the gel fraction was measured again. Despite the aggressive hydrolytic conditions employed, these membranes retained gel fractions close to 90% (cf. Table S4, SI). Therefore, despite the lower temperature, a high crosslinking efficiency, resulting in hydrolysis-resistant crosslinks, can be achieved by extending the crosslinking time.

Figure 3A shows ATR-FTIR spectra of MMM30 and IcMMM30 membranes. Two main spectral features confirm the chemical transformations occurring. First, the signals associated to the carboxylic acid -OH and C=O stretches at 3500 cm<sup>-1</sup> and 1720 cm<sup>-1</sup> are depressed in the thermally treated sample, indicating some degree of decarboxylation occurs during treatment. Moreover, peaks located at 1440-1480 cm<sup>-1</sup> in IcMMM30 experience a 25 cm<sup>-1</sup> blueshift to 1465-1513 cm<sup>-1</sup>, while the C-O-C stretch at 1004 cm<sup>-1</sup> present in the MMM30 sample becomes significantly diminished along with the appearance of a new peak at 975 cm<sup>-1</sup> in the IcMMM30 sample. The large blueshift in the stretching region between 1440-1480 cm<sup>-1</sup> in the IcMMM30 sample, which includes C=C aromatic stretching, C-O stretching, and methylene bridge -CH<sub>2</sub> bending modes [57,68–70], is likely the result of changes to the substitution pattern on the aromatic benzodioxin moieties in the CPIM backbone or carbon-carbon bond disruption between the methylene bridge and spiro center. Notably, the bending vibration of the methyl groups at 1369 cm<sup>-1</sup> [60] is unaffected by thermal treatment, which indicates that any C-C bond scission is prone to occur close to the spiro center in the PIM backbone. Changes in the C-O-C stretch in the thermally treated sample further confirm the significant change in the substitution pattern on the aromatic moieties, namely, loss of acid groups or formation of the aromatic C-C crosslinks that typically occur during decarboxylation crosslinking [31,65].

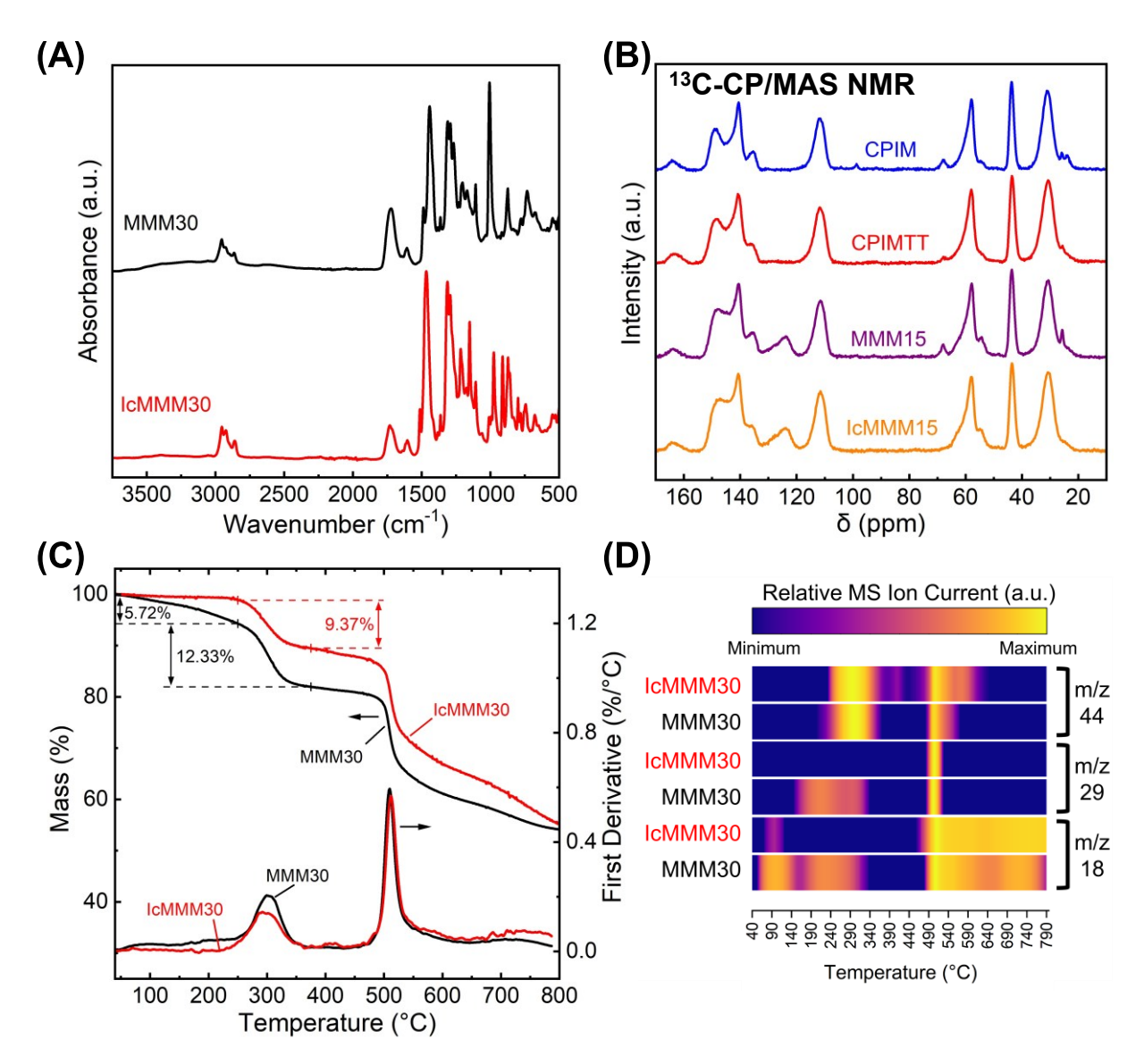


**Figure 3.** Study of the thermal treatment by (A) FTIR-ATR of MMM30 and IcMMM30, (B) <sup>13</sup>C-CP/MAS NMR spectra of CPIM, CPIMTT, MMM30 and IcMMM30, (C) TGA mass loss analysis of MMM30 and IcMMM30, and (D) mass spectrometry signals corresponding to the TGA experiments in (C).

<sup>13</sup>C CP/MAS NMR spectra were collected on both untreated and thermally treated analogues of CPIM and MMM15 (Figure 3B). Since the thermal crosslinking process occurs due to the CPIM chemistry, 15 wt. % loading was used instead of 30% to maximize the signal due to changes happening to the CPIM. The signals expected for the CPIM structure agree with the <sup>13</sup>C NMR

presented in section 4.1 and signals corresponding to the aromatic carbons in the triptycene-isatin PPN are observed at 123 and 145 ppm as a distinct peak and shoulder contribution, respectively. Additionally, the methine bridge in the triptycene group appears at 54 ppm [42]. No significant changes in the peaks corresponding to the carbon skeleton in either CPIM or the PPN are observed to occur due to the thermal annealing process. This is likely due to changes in the substitution pattern producing signals that are overshadowed by already extant signals, or that subtle changes are occurring that are beyond the limit of detection of the instrument.

Notable shoulder contributions to the aliphatic carbons in the CP/MAS spectra appear at 67 and 25 ppm in the untreated samples. These signals either greatly diminish or completely disappear upon thermal treatment. These align well with the expected <sup>13</sup>C signals for THF—the casting solvent for the samples—shown in Figure 2E. However, all samples used for the CP/MAS analysis were dried at 110°C for 12h under vacuum before analysis, so it seems unlikely that THF, with a boiling point of 66°C, would remain occluded in the samples after this treatment. Further, the signal is still weakly present in the CPIMTT sample, which was treated at 200°C for 24 hours under vacuum. These apparently contradictory observations are explained by considering the interaction between the casting solvent, THF, and the residual sulfuric acid present in the CPIM after synthesis that was detected using elemental analysis (cf. Table 1). As mentioned earlier, a dilute acid wash is applied in the final step of the CPIM synthesis to retain the protonated acid form, and the residual sulfuric acid likely interacts with THF in the casting solutions for the membranes to form short-chain oligomers of THF (i.e., poly(THF)), which have <sup>13</sup>C signals that correspond to those seen in Figure 3B [71]. Sulfuric acid is a common catalyst in ring-opening polymerizations (ROPs) and is known to catalyze the cationic ROP of THF, leading to the production of oligomeric species with molecular weights < 1000 Da [72]. These oligomeric polyTHF species will have a significantly higher boiling point than THF and have been shown to degrade under inert conditions at the temperatures employed [71,73]. Considering the small amount of sulfuric acid present and the relatively weak signals seen in the CP/MAS, these polyTHF species are likely removed during thermal treatment through a combination of thermal degradation and evaporation processes. The effect of the poly(THF) species on the degree of crosslinking or hydrolytic stability of the crosslinked membranes was found to be minimal. Specifically, CPIMTT membranes boiled in water and cast from either THF or DMF exhibited gel fractions close to 90%

(cf. Table S4, SI). Possible effects of poly(THF) on membrane transport properties are discussed in Section 4.4.

Further confirmation of the chemical crosslinking mechanism is provided by the TGA-MS measurements on MMM30 and IcMMM30 membranes shown in Figure 3C-D. PPN, due to its thermal stability, should not contribute significantly to the observed differences, and TGA of neat CPIM closely reflects that of the MMM30 sample. TGA of neat CPIM and PPN are discussed in the SI, Section S15. Thus, the different mass losses exhibited by the two samples should originate from processes occurring during the thermal treatment process. Notably, the untreated MMM30 sample shows a sloping mass loss of 5.72% from 100-250°C that is not present in the IcMMM30 sample. As both samples were dried at 110 °C overnight in a vacuum oven before analysis, it is unlikely that this difference in mass loss is due to residual moisture or solvent and is instead a combination of low-temperature decarboxylation and removal of the poly(THF) that occurs during thermal treatment.

The smaller area of the first derivative decarboxylation peak for the thermally treated sample, relative to the untreated sample, confirms the partial decarboxylation occurring during thermal treatment that was also seen in the FTIR analysis. By comparing the mass losses from 250 to 375°C, it appears that the MMM30 membrane loses about 3% more mass during decarboxylation. For a fully carboxylated CPIM, complete decarboxylation of this sample would result in a 12.46% mass loss (after adjusting for the 30 wt. % PPN content) [15]. After accounting for the 92.0% hydrolysis of the CPIM found from elemental analysis, this 3% mass loss difference indicates that approximately 25.8% of acid groups are lost during thermal treatment.

In the mass spectrometry signals (cf. Figure 3D), differences were observed primarily in the lower temperature degradation products. First, a m/z = 29 signal was observed from the MMM30 sample from 140-350°C that is not observed from IcMMM30. This ion fragment was assumed to be associated with the ethyl ion fragment originating from either the evolution or decomposition of THF or poly(THF) oligomers, but would also be produced in the degradation of the main-chain PIM backbone [74,75]. The m/z = 29 signal presents as a bimodal evolution in MMM30 with peaks centered at 200 and 300°C, which suggests that multiple pathways could be producing this signal. Minor degradation of the aliphatic C-C bonds in the aliphatic moieties of the PIM backbone could also contribute to the observed degradation behavior, as changes in these peaks were observed in the FTIR spectra (cf. Figure 2C). The absence of this signal from IcMMM30 at these

lower temperatures provides direct confirmation that these species are efficiently removed during thermal treatment. For the m/z = 18 signal, which corresponds to water evolution, some differences between MMM30 and IcMMM30 are observed as well. While both samples exhibit an evolution near  $100^{\circ}$ C, typical of physi-sorbed moisture, the untreated MMM30 sample exhibits a secondary water evolution spanning from  $140\text{-}350^{\circ}$ C. This behavior is also consistent with the same degradation pathways discussed for the m/z = 29 signal, in addition to the expected water production as a result of condensation of adjacent acid groups to anhydride groups [31,65]. Little to no changes were observed in the production of carbon dioxide between the two samples (m/z = 44).

Based on the observed decarboxylation, high gel fractions, and hydrolysis resistant crosslinks, it seems that the conventional decarboxylation pathway, in which a free radical process induces degradation of anhydride species leading to the formation of C-C crosslinks, is occurring in our materials. One interesting feature of this pyrolytic degradation is the ability to sustain crosslinks to external aromatic substrates, rather than just between two acid-containing sites. Eskay et al. studied in depth this chemistry and found that aromatic acids grafted to naphthalene by a free radical process [65]. Thus, since this degradative pathway has been established to be occurring in the samples studied, some degree of grafting between CPIM and the aromatic substrates on the PPN should take place. The various crosslinking pathways leading to C-C crosslinks in the membrane are illustrated in Figure 4A, with the resulting hypothesized inter-crosslinked structure portrayed in Figure 4B. The effect of inter-crosslinking on the membrane plasticization resistance and transport properties is discussed in Section 4.5.

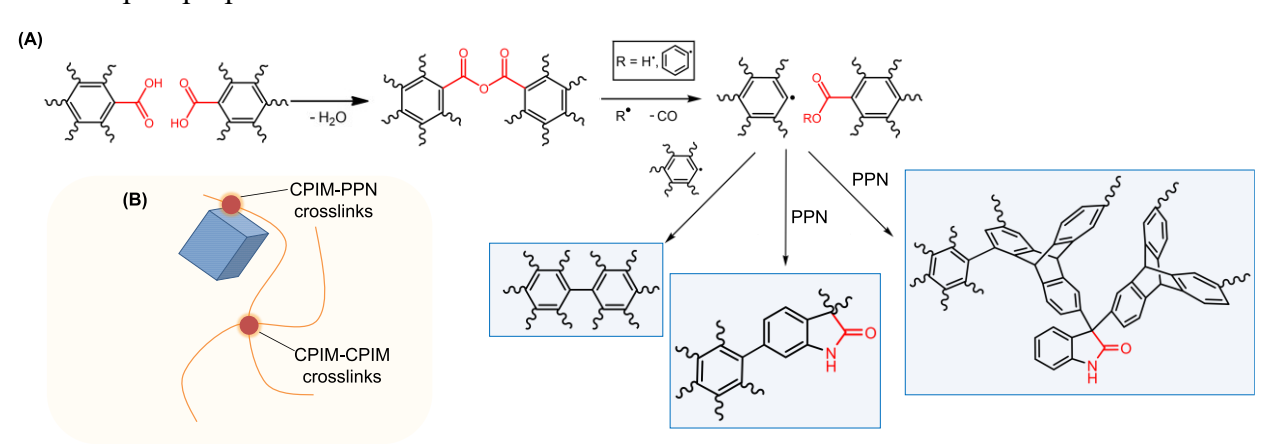


**Figure 4.** (A) Proposed crosslinking mechanism, with the final C-C crosslinked structures highlighted in blue. (B) Artwork depicting the structure of IcMMM30.

4.3 Pure Gas Permeability and Selectivity. Pure gas H<sub>2</sub>, CH<sub>4</sub> and CO<sub>2</sub> permeabilities at 35°C in CPIM, CPIMTT, MMM30, and IcMMM30 are tabulated in section S17, SI. CH<sub>4</sub> and H<sub>2</sub> (cf., Figure S6, SI) permeability isotherms exhibit the dual mode behavior typical of glassy polymers, with a constant or monotonically decreasing permeability as a function of fugacity. In the case of CO<sub>2</sub>, the dual mode behavior is observed, in the entire pressure range, up to 50 atm, only for IcMMM30, while the other samples exhibit a clearly discernible upturn ascribed to plasticization. Details about the CO<sub>2</sub>-induced plasticization behavior are provided in Section 4.5.

Pure-gas H<sub>2</sub>/CH<sub>4</sub> selectivity at 35°C and 10 atm is shown, as a function of H<sub>2</sub> permeability, in an upper-bound plot in Figure 5A.

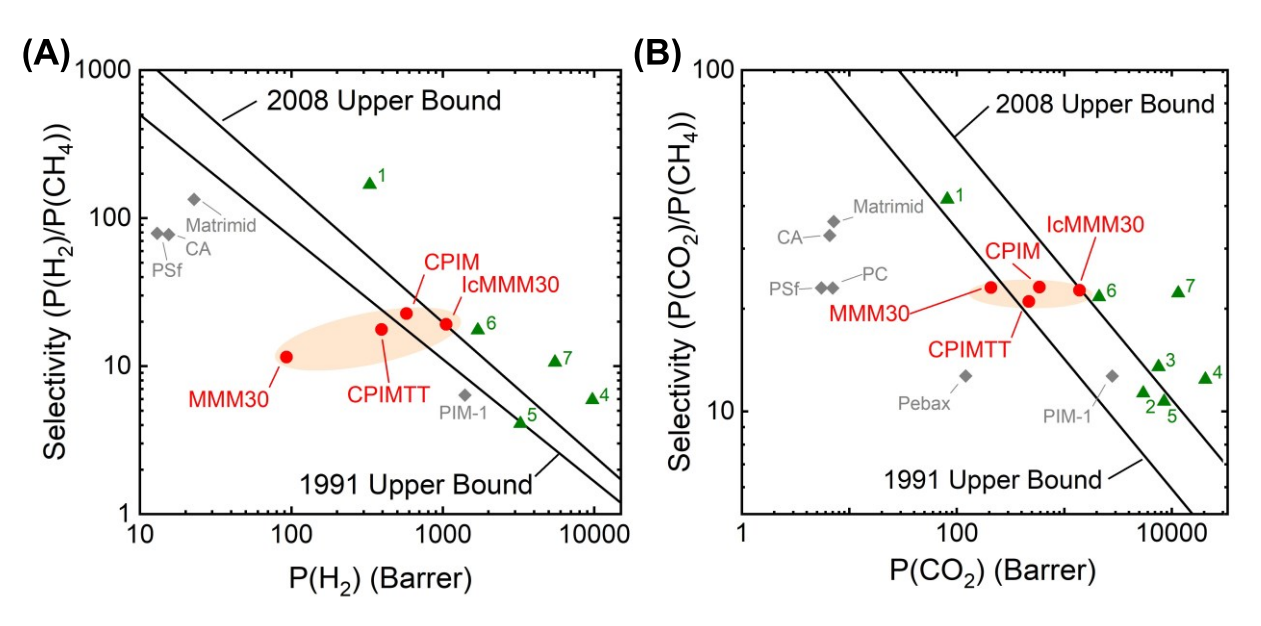


Figure 5. Upper bound plots for the (A) H<sub>2</sub>/CH<sub>4</sub> (35°C, 10 atm) and (B) CO<sub>2</sub>/CH<sub>4</sub> (35°C, 1 atm) gas pairs. State of the art polymer membranes are denoted in gray and include cellulose acetate (CA) [53], polysulfone (PSf) [76,77], polycarbonate (PC) [78], PIM-1 [15], Matrimid® [79,80], and Pebax [81]. Previously reported PIM-based composite membranes are shown as green triangles: 1- PIM-1/POSS [82], 2- PIM-1/CC3 [83], 3- PIM-1/COF(SNW-1) [84], 4- PIM-1/pDCX [85], 5- PIM-1/UiO-66-NH<sub>2</sub> [40], 6 - CPIM/UiO-66-NH<sub>2</sub> [40], 7 - CPIM/diacetyl biphenyl PPN [86].

H<sub>2</sub> permeability and H<sub>2</sub>/CH<sub>4</sub> selectivity decrease by 32% and 22%, respectively, upon thermal treatment of CPIM (i.e., CPIMTT). Upon blending with 30 wt. % triptycene-isatin PPN (i.e., MMM30), a further 84% decrease in the H<sub>2</sub> permeability and 49% decrease in the H<sub>2</sub>/CH<sub>4</sub> selectivity is observed relative to CPIM. However, after thermal treatment of MMM30, the resulting IcMMM30 experiences a >1,000% increase in the H<sub>2</sub> permeability and a 66% increase in selectivity with respect to its untreated analogue MMM30 membrane, with an overall performance lying on the 2008 upper bound. As shown in Figure 5B, quantitatively similar results were observed for the CO<sub>2</sub>/CH<sub>4</sub> gas pair at 35°C and 1 atm. To note, data at 1 atm instead of 10 atm were used for the CO<sub>2</sub>/CH<sub>4</sub> upper bound to avoid any artifacts due to plasticization of CPIM, CPIMTT and MMM30. To put these results in a broader perspective, in Figures 5A-B, the performance of the IcMMM30 is compared to that of state-of-the-art materials and, including other spirocyclic polymers.

As shown by Lozano et al., blending triptycene-isatin PPN with polyimides with no thermal treatment leads to an increase in permeability and a moderate drop in selectivity, while a marked permeability drop is observed in MMM30 relative to CPIM [43]. As discussed in Section 4.4, the ~65% CO<sub>2</sub> permeability decrease experienced by MMM30 relative to neat CPIM is ascribed to the presence of short-chain, oligomeric poly(THF) species, which are expected to partially occupy the PPN pores. Poly(THF) oligomers in MMM30, whose presence is confirmed by solid state <sup>13</sup>C CP/MAS NMR measurements, were found to be removed efficiently by the thermal treatment at 200°C. Interestingly, gas permeability in CPIM, which also contains poly(THF), is not significantly hindered, as it closely matches previously reported values [15]. This fact suggests that poly(THF) preferentially occupies the PPN pores, more than the CPIM excess free volume pockets. More investigation on this phenomenon is underway. To shed light on the fundamental origin of the observed transport behavior, in section 4.4 gas permeability and selectivity were broken into their elementary sorption and diffusion contributions.

4.4 Pure Gas Sorption, Diffusion, and Dual Mode Modeling. Pure gas CO<sub>2</sub> and CH<sub>4</sub> sorption isotherms at 35°C in CPIM, CPIMTT, MMM30 and IcMMM30 are shown in Figures 6A-B as a function of fugacity in the contiguous external gas phase. Fugacity was calculated using the Peng-Robinson equation of state, and experimental uncertainties were calculated using linear error propagation [54]. H<sub>2</sub> sorption in these polymers is below the limit of experimental detectability, therefore it could not be measured. Finally, diffusion coefficients were calculated from experimental permeability and sorption data, via the solution-diffusion model.

CO<sub>2</sub> and CH<sub>4</sub> sorption in CPIMTT are 59% and 44% higher than in neat CPIM, respectively. Similar increases in the sorption capacity have been reported in the literature for acid-containing polymers upon thermal decarboxylation [37]. More in general, thermal decarboxylation of polymers produces two competitive effects. First, it allows a more densely packed structure to form, due to free volume collapse (i.e., accelerated physical aging), which causes a moderate decrease in penetrant solubility; secondly, removing bulky -COOH groups creates new microcavities, increasing Langmuir's mode sorption. Sorption isotherms in Figures 6A-B, and solubility coefficients in Figure 6C indicate that the latter effect largely overwhelms the former. More specifically, the dual mode analysis, summarized in Figures 6A-B and Table 2, suggests that, for both CO<sub>2</sub> and CH<sub>4</sub>, CPIMTT exhibits larger values of the Langmuir sorption capacity,  $C'_H$ , relative to CPIM, which confirms that thermal decarboxylation enhances, at least for these materials, sorption capacity. However, as discussed in the previous section, gas permeability decreases upon thermal treatment of CPIM, indicating that a parallel decrease of diffusivity must take place (cf., Figure 6D). To explain this behavior on a more fundamental basis, diffusivity was broken into its Henry's (i.e.,  $D_D$ ) and Langmuir's (i.e.,  $D_H$ ) contributions using the partial immobilization model (cf. Section S18, SI). The dual mobility modeling points out two main effects. First, for both penetrants and in both CPIM and CPIMTT,  $D_H$  is one order of magnitude lower than  $D_D$  (cf., Table 2). Moreover, in CPIMTT, the relative contribution of Langmuir's mode diffusion to the total overall diffusivity (i.e.,  $F = {}^{D_H}/{}_{D_D}$ , cf., Table 2) is almost doubled relative to CPIM, which explains why gas diffusivity and permeability decrease upon thermal treatment of CPIM. This physical picture is also consistent with the increase of the Langmuir's sorption capacity,  $C'_H$ , observed in CPIMTT relative to CPIM, which causes sorption to increase upon thermal treatment.

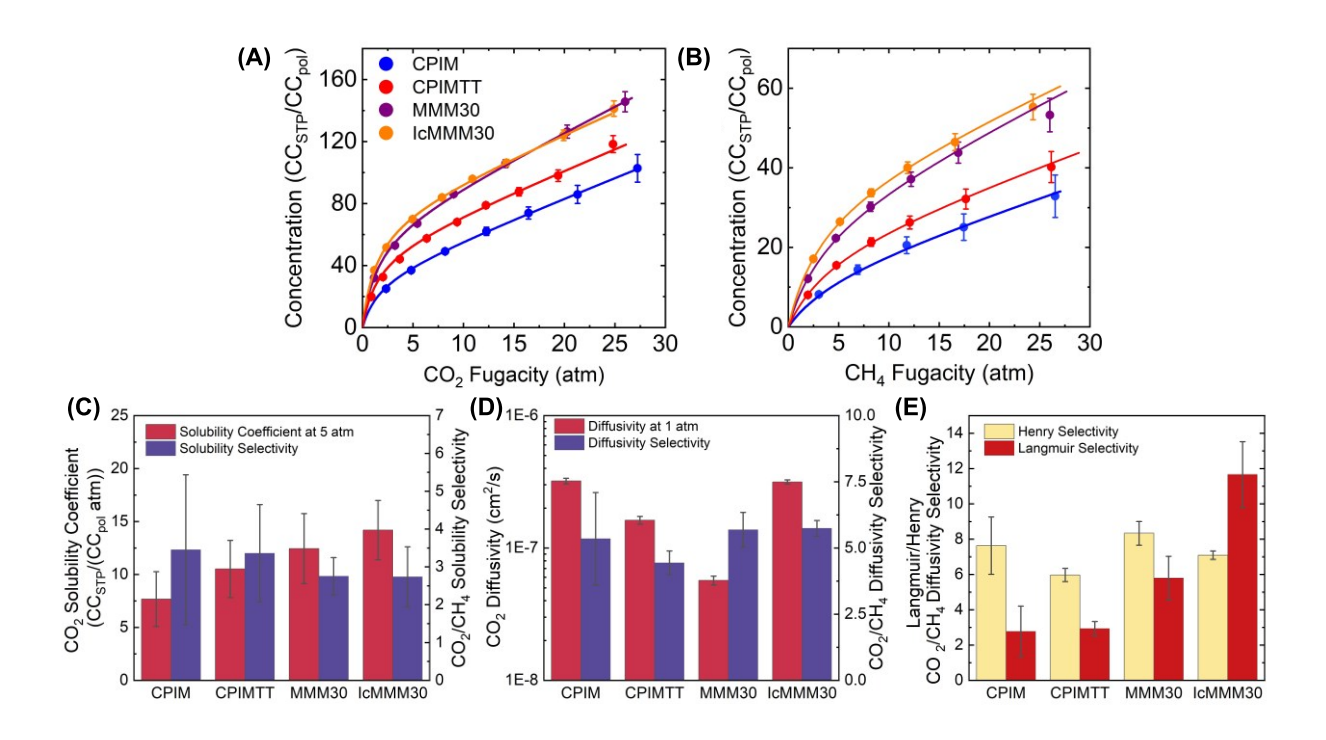


Figure 6. Pure (A)  $CO_2$  and (B)  $CH_4$  sorption isotherms in CPIM, CPIMTT, MMM30 and IcMMM30. (C) Pure  $CO_2$  solubility coefficients and  $CO_2/CH_4$  ideal solubility-selectivity. (D) Pure  $CO_2$  diffusivity and  $CO_2/CH_4$  ideal diffusivity-selectivity. (E) Henry's and Langmuir's mode  $CO_2/CH_4$  diffusivity-selectivity (i.e.,  $D_D^{CO_2}/D_D^{CH_4}$  and  $D_H^{CO_2}/D_H^{CH_4}$ ).

To avoid mathematical artifacts and enhance the physical meaning of the parameters, the dual mode fit of sorption data was run by constraining the slope of  $ln(k_D)$  and ln(b) versus gas critical temperature to be the same as the slope of ln(S) versus gas critical temperature at 10 atm, according to the procedure recommended by Smith et al. [15,87].

Incorporating 30 wt. % PPN causes a 37% increase in  $CO_2$  sorption in MMM30 relative to CPIM, which is consistent with the much larger surface area exhibited by PPN relative to CPIM, as shown by BET measurements ( $S_{BET}(PPN) = 695 \text{ m}^2/\text{g} > S_{BET}(CPIM) = 373 \text{ m}^2/\text{g}$ ). Notably, this fact indicates that CPIM is not extensively infiltrating and occupying the PPN's pores, thus ruling out any possible polymer interlocking through the PPN's porosity. This picture is also supported by simple geometric considerations. More specifically, the PPN cavities' diameter is less than 0.7 nm [42], while the cross-sectional diameter of bulky CPIM is expected to be 0.75 nm or higher, based on the end-to-end distance of the carbonyl oxygens in terephthalic acid. The lack of CPIM

interlocking through the PPN porosity is also confirmed by the plasticization study, as discussed in section 4.5.

However, gas permeability in MMM30 is lower than in CPIM, which can only be caused by a parallel decrease in diffusivity (cf., Figure 6D). The CO<sub>2</sub> diffusion coefficient in MMM30 is almost six times lower than in CPIM due to *i*) the presence of triptycene units, which, as previously shown, slow down gas diffusion [50] and *ii*) oligomeric poly(THF) partially occupying the PPN pores, as discussed in Section 4.2. For both CO<sub>2</sub> and CH<sub>4</sub>, MMM30 exhibits lower values of  $D_D$  and  $D_H$  relative to neat CPIM. In the case of  $D_H$ , a larger decrease is observed for CH<sub>4</sub> (-82%), which is a bulkier penetrant relative to CO<sub>2</sub> (-70%).

Finally, IcMMM30 experiences no significant changes in gas sorption relative to MMM30, especially in the case of CO<sub>2</sub>. In the case of CH<sub>4</sub> a slight increase is apparent within the experimental uncertainty. Therefore, the large permeability increase exhibited by IcMMM30 relative to the non-thermally treated MMM30 is essentially due to the diffusion behavior. This fact is confirmed by the simultaneous increase in  $D_H$  and  $D_D$  observed in IcMMM30 for both penetrants relative to MMM30. Interestingly, if we take CPIM as the basis of comparison, the larger permeability exhibited by IcMMM30 mirrors its larger gas sorption capacity relative to CPIM, while diffusivity is essentially the same for the two materials. In other words, while sorption tends to increase in the order CPIM < CPIMTT < MMM30 ≈ IcMMM30, diffusion first decreases in the order CPIM > CPIMTT > MMM30, and then for IcMMM30 it recovers a similar value as for the original CPIM sample. As shown in Table 2, the increase in CO<sub>2</sub> sorption observed from CPIM to IcMMM30 is due to a 114% increase in the Langmuir sorption capacity,  $C'_H$ , while the Henry's mode contribution,  $k_D$ , exhibits a much smaller increase of 8.14%. Therefore, the increased sorption capacity exhibited by IcMMM30 relative to the baseline material, CPIM, is likely caused by i) the elimination of bulky -COOH groups, and ii) the additional surface area provided by the microporous PPN.

 $D_D$  and  $D_H$  values for CO<sub>2</sub> in IcMMM30 recover and slightly surpass the values observed in CPIM. In the case of CH<sub>4</sub>,  $D_D$  recovers almost the same value as for CPIM, while  $D_H$  surpasses the value observed in CPIM by 170%. This trend is consistent with the increase in Langmuir capacity offered by the PPN and with the efficient removal of poly(THF) and subsequent pore activation of the PPN, as discussed in the structural analysis. Overall, CO<sub>2</sub>/CH<sub>4</sub> diffusion selectivity increases by

7.3% in IcMMM30 relative to CPIM, while solubility-selectivity experiences a 4.4% decrease. Fractional free volume (FFV) calculations confirm this physical picture, with both CPIM and IcMMM30 exhibiting essentially similar FFVs of 21.0% (cf. Table S3, SI). More details on the role and interpretation of FFV are provided in the SI, Section S4.

Interestingly, while Henry's  $CO_2/CH_4$  diffusion selectivity (i.e.,  $D_D^{CO_2}/D_D^{CH_4}$ ) remains approximately constant among samples, Langmuir's  $CO_2/CH_4$  selectivity (i.e.,  $D_H^{CO_2}/D_H^{CH_4}$ ) increases in the order CPIM  $\approx$  CPIMTT < MMM30 < IcMMM30. This behavior is primarily attributed to the presence of triptycene units in the PPN structure, which contain configurational free volume (i.e., the intramolecular spaces within triptycene moieties), providing an effective enhancement of the size sieving ability in specifically the Langmuir mode of transport, in accordance with the mechanism discussed by Box et al. [50].

In conclusion, the observed increase in  $CO_2$  permeability in the order MMM30 < CPIMTT  $\approx$  CPIM < IcMMM30 is due to increases in both  $CO_2$  sorption and diffusivity. The slight increase in diffusivity selectivity is offset by a small decrease in sorption selectivity, which renders the overall  $CO_2/CH_4$  permeability selectivity essentially constant across samples.

**Table 2**: Summary of the dual mode model fittings. Error bars were obtained using the Jackknife resampling technique. Parameters were fit with respect to penetrant fugacity and were constrained using the technique reported in [15,87].

sample	gas	$k_D$	$C_H'$	b	$D_D \times 10^7$	$D_H \times 10^8$	F
		$(CC_{STP}/(CC_{pol} atm))$	$(CC_{STP}/CC_{pol})$	(atm <sup>-1</sup> )	$(cm^2/s)$	$(cm^2/s)$	1
СРІМ	$CO_2$	$2.58 \pm 0.04$	$34.0 \pm 0.98$	$0.597 \\ \pm 0.03$	$15.57 \pm .03$	$3.4 \pm 0.3$	0.022
	CH <sub>4</sub>	$0.81 \pm 0.17$	$14.4 \pm 6.4$	0.192 ± 0.040	$2.0 \pm 0.4$	$1.2 \pm 0.6$	0.060
СРІМТТ	$CO_2$	$2.68 \pm 0.1$	$50.7 \pm 2.0$	$\begin{array}{c} 0.680 \\ \pm 0.043 \end{array}$	$9.8 \pm 0.4$	$4.4 \pm 0.4$	0.045
	CH <sub>4</sub>	$0.88 \pm 0.04$	21.3 ± 1.2	$0.226 \\ \pm 0.012$	$1.64 \pm 0.08$	$1.5 \pm 0.2$	0.092
<i>MMM30</i>	$CO_2$	$3.26 \pm 0.10$	$64.5 \pm 3.0$	$\begin{array}{c} 0.682 \\ \pm 0.070 \end{array}$	$4.0 \pm 0.2$	$1.1 \pm 0.2$	0.027

	CH <sub>4</sub>	$1.20 \pm 0.09$	$29.5 \pm 2.5$	$0.257 \\ \pm 0.015$	$0.48 \pm 0.03$	$0.18 \pm 0.02$	0.038
IcMMM30	$CO_2$	$2.79 \pm 0.050$	73 ± 1	$0.713 \\ \pm 0.028$	$25.4 \pm 0.5$	$11.0 \pm 0.5$	0.043
	CH4	$1.10 \pm 0.02$	$34.7 \pm 0.7$	$0.286 \\ \pm 0.007$	$3.6 \pm 0.1$	$0.9 \pm 0.1$	0.026

4.5 CO<sub>2</sub>-induced Plasticization Study. A dedicated plasticization study was run by measuring, in the series of four materials, CO<sub>2</sub> permeability at 35°C up to 50 atm. In Figure 7A, the plasticization behavior of non-thermally treated samples, i.e., CPIM and MMM30, is shown as a function of pressure. CPIM plasticizes at about 7 atm, which is in reasonable agreement with previously reported data [15]. Recently, Matesanz-Niño et al. showed that hydrogen bonding between an acid-containing polyimide and triptycene-isatin PPN was able to suppress CO<sub>2</sub>-induced plasticization up to 30 atm, thus it was hypothesized that hydrogen bonding between the -COOH groups in CPIM and amide groups in the PPN may lead to plasticization resistance [88]. In striking contrast with the expected behavior, MMM30 suffers from an even stronger plasticization propensity relative to CPIM, with the onset of plasticization showing up at about 4 atm. The stronger plasticization propensity exhibited by MMM30 relative to neat CPIM indicates that i) the polymer-filler physical interactions (e.g., CPIM threading through or interlocking with the PPN) is not occurring, which mirrors the results of the sorption-diffusion study discussed in the previous section, and that ii) significant CPIM-PPN chemical interactions, such as hydrogen bonding, is not occurring in non-thermally treated mixed matrices.

The plasticization behavior of thermally treated samples is shown in Figure 7B. Thermally treated CPIM, i.e., CPIMTT, plasticizes at about 15 atm CO<sub>2</sub>. The enhanced plasticization resistance exhibited by the latter polymer relative to CPIM is consistent with its crosslinked structure resulting from thermally induced decarboxylation. Remarkably, IcMMM30 does not exhibit any detectable CO<sub>2</sub>-induced plasticization up to 50 atm, which places this material among the best reported in terms of plasticization resistance. As shown in Figure 7C, the plasticization resistance exhibited by IcMMM30 is comparable only to that of a handful of other polymeric membrane materials, such as membranes fabricated with branched MOFs [89], polymers with ultra-rigid sidechain porosity [90], and advanced crosslinked polyimides exhibiting π-stacking interactions

[37]. It should be noted that, for this test, each CO<sub>2</sub> pressure was held for 24h, thus IcMMM30 was exposed to high pressures of CO<sub>2</sub> for 14 days by the end of the experiment, which makes its plasticization resistance even more remarkable. Interfacial polymer-PPN crosslinking is responsible for the excellent plasticization resistance exhibited by IcMMM30. Previously, Jiang et al. reported high plasticization resistance in membranes fabricated by mixing poly(ethylene oxide) with UiO-66 MOFs exhibiting polymer-filler crosslinking relative to composites with no interfacial crosslinking [91], a result that confirms the trend observed in this study.

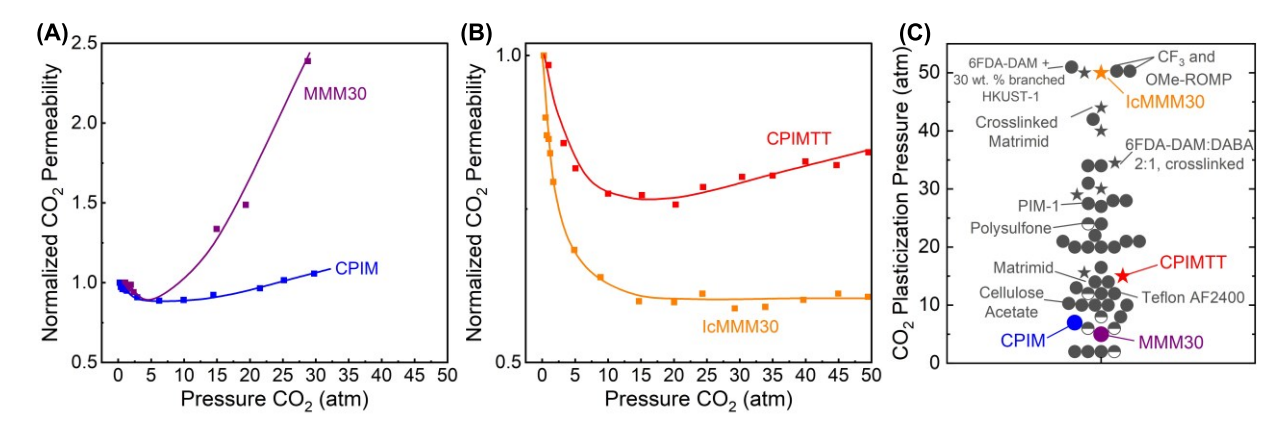
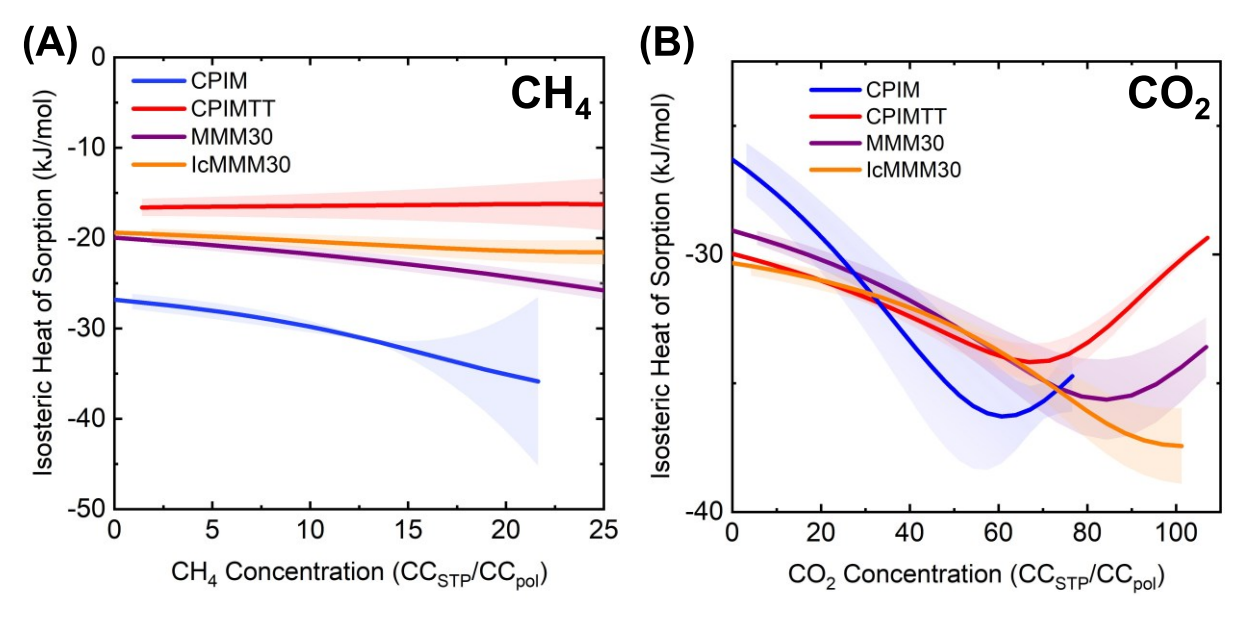


Figure 7.  $CO_2$  plasticization test for (A) untreated samples (i.e., CPIM and MMM30) and (B) thermally treated samples (i.e., CPIMTT and IcMMM30). (C) Review of  $CO_2$  plasticization pressures for the materials reported in this study, as well as state of the art materials. Stars represent crosslinked films, and half-filed symbols are thin films (< 1  $\mu$ m). Data for non-crosslinked film are from ref. [90], and data for crosslinked and mixed-matrix films are tabulated in the SI, Table S9.

While polymer-filler crosslinking seems to be the key factor, any effects due to simple physical interactions between CPIM and the PPN should be ruled out. The thermal treatment was performed at 200°C, which is well below the glass transition temperature of PIM materials (i.e., > 400°C) [92]. Additionally, DSC measurements confirmed that none of the studied samples exhibited glass transitions or any relaxations below 300°C, as shown in Section S7, SI. This fact, in conjunction with the rigidity exhibited by CPIM and its bulky structure, would exclude the occurrence of any CPIM interlocking or threading through the cavities of the PPN (whose microcavities are primarily <0.7 nm in diameter [42]) as a result of thermal treatment.

The plasticization resistance exhibited by IcMMM30 is confirmed, from a thermodynamic standpoint, by the analysis of the isosteric heats of sorption (cf., Figure 8). Being a non-polar, nonplasticizing gas, CH<sub>4</sub> should exhibit almost no variations in the energetics of interaction with the polymer phase, and this is seen to be the case, where the isosteric heat of CH<sub>4</sub> sorption is, within the experimental uncertainty, constant as a function of CH<sub>4</sub> concentration in the polymer (cf., Figure 8A). In contrast, CO<sub>2</sub>, which is a more condensable quadrupolar gas, is known to plasticize polymers. As shown in Figure 8B, the isosteric heat of CO<sub>2</sub> sorption in CPIM, CPIMTT and MMM30 exhibit a well detectable minimum as a function of CO<sub>2</sub> concentration in the polymer. The presence of this minimum indicates that positive deformation work is required to accommodate additional CO<sub>2</sub> molecules in the polymer by pulling apart polymer chains. Interestingly, the concentration at which the minimum appears substantially increases by moving from CPIM to CPIMTT as a consequence of crosslinking. Remarkably, the CO<sub>2</sub> isosteric heat of sorption in IcMMM30 does not exhibit any minimum, as it monotonically decreases with increasing CO<sub>2</sub> concentration. This fact indicates that little or no deformation work is being provided to pull polymer chains apart for accommodating additional penetrant molecules in this sample, which mirrors the results of the plasticization study, confirming that strong, irreversible polymer-filler inter-crosslinking is the key factor leading to superior plasticization resistance. Thus, engineering the polymer-filler interface with covalent bonds appears to be a viable strategy to simultaneously tackle the problems of membrane permeability, selectivity, and stability without adding too much complexity to the material synthesis or membrane fabrication process.



**Figure 8.** Isosteric heats of sorption for (A) CH<sub>4</sub> and (B) CO<sub>2</sub> in CPIM, CPIMTT, MMM30, and IcMMM30. Continuous lines denote experimentally determined values, and the shaded region surrounding each line is the experimental error determined, at each concentration, via linear error propagation and the standard error of linear regression [93].

To better highlight the excellent stability exhibited by IcMMM30 and put it in a broader perspective, in Table S9, SI, we compare the plasticization pressures (i.e., the pressure at which a minimum in CO<sub>2</sub> permeability is observed) across several polymers. Although comparing each polymer's plasticization propensity on a pressure basis is easy to do, it is more interesting, from a fundamental perspective, to compare the plasticization onset across materials at a given number of CO<sub>2</sub> molecules accommodated in the polymer matrix (i.e., at a given concentration), as shown in Table 3.

**Table 3:** Comparison of the pressures, permeabilities, and concentrations at which CO<sub>2</sub>-induced plasticization occurs in CPIM, CPIMTT, MMM30, IcMMM30 and state of the art materials. Literature data are taken from ref. [94].

polymer	CO <sub>2</sub> plasticization pressure (atm)	CO <sub>2</sub> permeability at plasticization (Barrer)	CO <sub>2</sub> concentration at plasticization (CC <sub>STP</sub> /CC <sub>pol</sub> )	temperature (°C)
CPIM	7	546 ± 14	45 ± 2	35
CPIMTT	15	<i>368</i> ± <i>16</i>	83 ± 2	35
<i>MMM30</i>	5	$196 \pm 4$	$66 \pm 4$	35
IcMMM30	> 50	$976 \pm 26$	> 193 ± 2	35
Polysulfone	34	3.6	47	23
<i>Matrimid</i> <sup>®</sup>	12	4.8	47	22
P84	22	0.92	48	23
Cellulose acetate	11	6	31	27
Cellulose triacetate	10	7.3	31	24

All polymers presented in this study, apart from the neat CPIM, plasticize at higher CO<sub>2</sub> concentrations relative to previously reported polymers, indicating that PIM derivatives provide an excellent platform of materials to design highly stable membranes. Interestingly, MMM30, which is the lowest performance material among those studied in this work (cf. Figure 7), exhibits a much better stability when its performance is evaluated on concentration basis. Specifically, MMM30 plasticizes at a CO<sub>2</sub> content of about 66 CC<sub>STP</sub>/CC<sub>pol</sub>, while P84 polyimide, one of the most rigid materials used for organic solvent separations, plasticizes at a CO<sub>2</sub> content of 48 CC<sub>STP</sub>/CC<sub>pol</sub>. This comparison is useful to put in broader perspective our results and indicates that comparing plasticization propensity on solubility basis is formally more correct than pressure-based comparisons.

Data in Table 3 are summarized in Figure 9, where plasticization CO<sub>2</sub> permeability is compared across polymers in a 3D plot, as a function of plasticization pressure and plasticization CO<sub>2</sub> concentration. Remarkably, IcMMM30 stands out among state-of-the-art materials, exhibiting, simultaneously, no plasticization up to 50 atm, high plasticization CO<sub>2</sub> permeability, and superb CO<sub>2</sub> plasticization concentration.

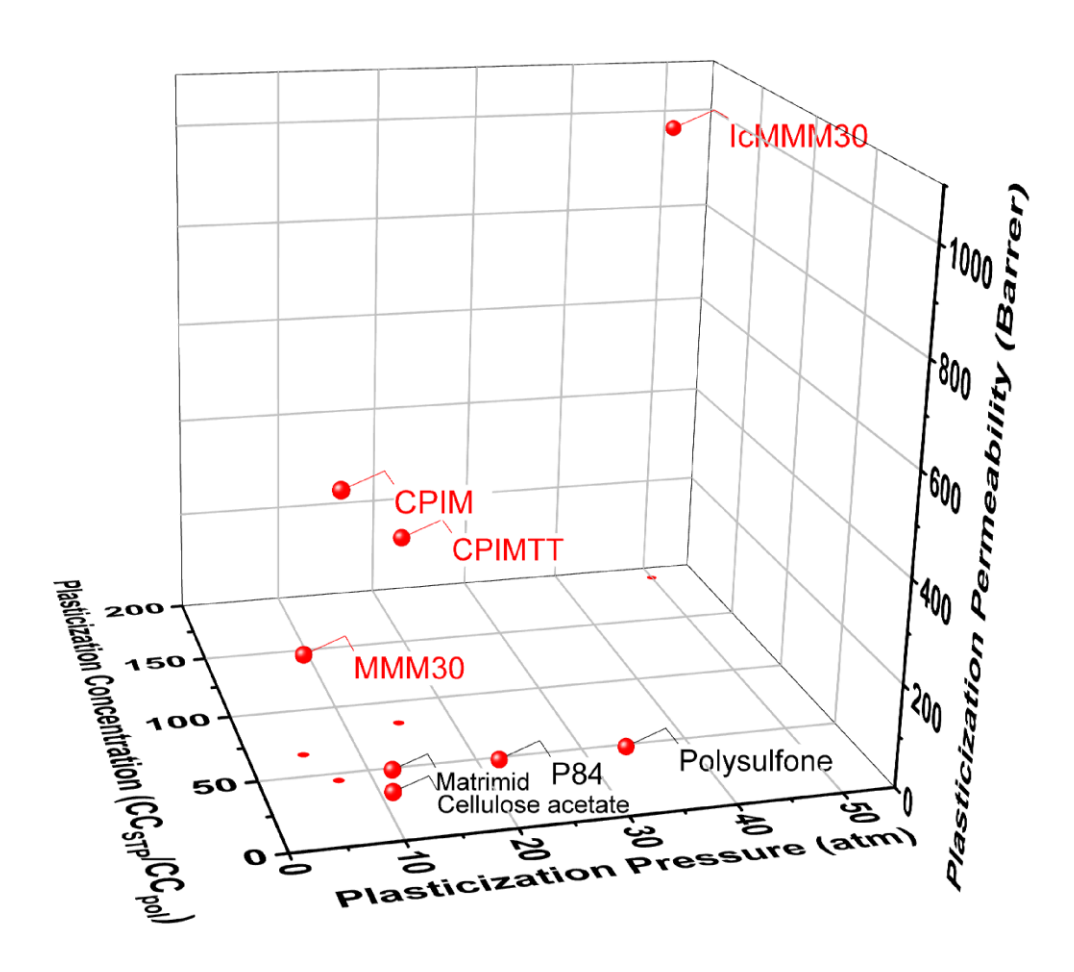


**Figure 9.** Plasticization  $CO_2$  permeability vs. plasticization pressure and plasticization  $CO_2$  concentration in several glassy polymers of interest in membrane separations. IcMMM30 outperforms other materials in all three axes.

## 5. Conclusions

Free-standing, mechanically robust inter-crosslinked mixed matrix membranes (IcMMMs) based on carboxylated polymer of intrinsic microporosity-1 (CPIM) and triptycene-isatin porous polymer networks (PPNs) were synthesized and characterized. Mutual polymer-filler crosslinking,

through a free-radical decarboxylation mechanism, was accomplished via a mild thermal treatment at 200°C under vacuum for 24h. It was shown that the main compositional changes resulting from the crosslinking process were minor decarboxylation, removal of low-molecular weight contaminants, and formation of hydrolytically stable crosslinks. The resulting IcMMMs perform on the 2008 upper bound for a variety of gas separation applications and exhibit ultra-high stability against plasticization upon prolonged CO<sub>2</sub> exposure up to 50 atm.

To isolate and quantify the individual and synergistic contributions of physical vs chemical polymer-filler interactions to the IcMMMs' performance, their structure and properties were compared *vis-à-vis* with those of neat CPIM, thermally treated CPIM, and CPIM-PPN mixed matrix membranes. The individual and synergistic effects of PPN incorporation and thermal treatment were studied via a detailed structural and transport analysis to demonstrate that polymer-filler crosslinking is the key factor enabling simultaneously high permeability, high selectivity, and superior long-term stability against plasticization. It was shown that the high permeability and selectivity exhibited by IcMMM30 stem from its high sorption capacity, and Langmuir's size-sieving ability, respectively. Removal of the low-molecular weight contaminants was also found to have an activating effect on the IcMMMs. IcMMMs stand out in terms of plasticization CO<sub>2</sub> permeability, plasticization pressure, and plasticization CO<sub>2</sub> concentration relative to conventional rigid glassy polymers, such as polyimide P84, Matrimid<sup>®</sup>, cellulose acetate and polysulfone.

One advantage of the fabrication approach developed in this work, due to the lower crosslinking temperature employed relative to prior studies, is its compatibility with conventional thin-film composite support layers such as PDMS or PAN. Investigation on the plasticization, physical aging, mixed gas transport, and organic solvent transport characteristics of the newly synthesized materials in the form of thin film composite membranes is underway.

### **Acknowledgments**

Financial support from the US National Science Foundation (NSF) through the CAREER Program (Grant # 2043648, Interfacial Engineering) is gratefully acknowledged. This material is based upon work supported by the National Science Foundation Graduate Research Fellowship Program under Grant No. 10557390. Any opinions, findings, and conclusions or recommendations expressed in this material are those of the author(s) and do not necessarily reflect the views of the National Science Foundation. The thermogravimetric setup used in this study was supported by

the University of Oklahoma SEIP (Strategic Equipment Investment Program) Program. The Authors thank Dr. Margaret Eastman, at Oklahoma State University, for running the <sup>1</sup>H, <sup>13</sup>C, and <sup>13</sup>C CP/MAS measurements. Microscopy data collection was performed at the Samuel Roberts Noble Microscopy Laboratory, an OU Core Facility supported by the Vice President for Research and Partnerships. The Authors would like to thank Dr. Laura Matesanz-Niño at the University of Valladolid for running BET measurements.

#### References

- [1] D.S. Sholl, R.P. Lively, Seven chemical separations to change the world, Nature 532 (2016) 435–437. https://doi.org/10.1038/532435a.
- [2] J. Deng, Z. Huang, B.J. Sundell, D.J. Harrigan, S.A. Sharber, K. Zhang, R. Guo, M. Galizia, State of the art and prospects of chemically and thermally aggressive membrane gas separations: Insights from polymer science, Polymer 229 (2021) 123988. https://doi.org/10.1016/j.polymer.2021.123988.
- [3] M. Galizia, W.S. Chi, Z.P. Smith, T.C. Merkel, R.W. Baker, B.D. Freeman, 50th Anniversary Perspective: Polymers and Mixed Matrix Membranes for Gas and Vapor Separation: A Review and Prospective Opportunities, Macromolecules 50 (2017) 7809–7843. https://doi.org/10.1021/acs.macromol.7b01718.
- [4] L.M. Robeson, Correlation of separation factor versus permeability for polymeric membranes, Journal of Membrane Science 62 (1991) 165–185. https://doi.org/10.1016/0376-7388(91)80060-J.
- [5] B.D. Freeman, Basis of Permeability/Selectivity Tradeoff Relations in Polymeric Gas Separation Membranes, Macromolecules 32 (1999) 375–380. https://doi.org/10.1021/ma9814548.
- [6] L.M. Robeson, The upper bound revisited, Journal of Membrane Science 320 (2008) 390–400. https://doi.org/10.1016/j.memsci.2008.04.030.
- [7] B. Comesaña-Gándara, J. Chen, C. Grazia Bezzu, M. Carta, I. Rose, M.-C. Ferrari, E. Esposito, A. Fuoco, J. C. Jansen, N. B. McKeown, Redefining the Robeson upper bounds for CO 2 /CH 4 and CO 2 /N 2 separations using a series of ultrapermeable benzotriptycene-based polymers of intrinsic microporosity, Energy & Environmental Science 12 (2019) 2733–2740. https://doi.org/10.1039/C9EE01384A.
- [8] N.A. of S. Medicine Engineering, and, D. on E. and L. Studies, B. on C.S. and Technology, C. on a R.A. for a N.E. in S. Science, A Research Agenda for Transforming Separation Science, National Academies Press, 2019.
- [9] R. Swaidan, B. Ghanem, E. Litwiller, I. Pinnau, Physical Aging, Plasticization and Their Effects on Gas Permeation in "Rigid" Polymers of Intrinsic Microporosity, Macromolecules 48 (2015) 6553–6561. https://doi.org/10.1021/acs.macromol.5b01581.
- [10] R. Swaidan, B. Ghanem, M. Al-Saeedi, E. Litwiller, I. Pinnau, Role of Intrachain Rigidity in the Plasticization of Intrinsically Microporous Triptycene-Based Polyimide Membranes in Mixed-Gas CO2/CH4 Separations, Macromolecules 47 (2014) 7453–7462. https://doi.org/10.1021/ma501798v.
- [11] M.M. Merrick, R. Sujanani, B.D. Freeman, Glassy polymers: Historical findings, membrane applications, and unresolved questions regarding physical aging, Polymer 211 (2020) 123176. https://doi.org/10.1016/j.polymer.2020.123176.
- [12] K.P. Bye, V. Loianno, T.N. Pham, R. Liu, J.S. Riffle, M. Galizia, Pure and mixed fluid sorption and transport in Celazole® polybenzimidazole: Effect of plasticization, Journal of Membrane Science 580 (2019) 235–247. https://doi.org/10.1016/j.memsci.2019.03.031.
- [13] M. Huang, K. Lu, Z. Wang, X. Bi, Y. Zhang, J. Jin, Thermally Cross-Linked Amidoxime-Functionalized Polymers of Intrinsic Microporosity Membranes for Highly Selective Hydrogen Separation, ACS Sustainable Chem. Eng. 9 (2021) 9426–9435. https://doi.org/10.1021/acssuschemeng.1c02784.

- [14] R. Swaidan, B.S. Ghanem, E. Litwiller, I. Pinnau, Pure- and mixed-gas CO2/CH4 separation properties of PIM-1 and an amidoxime-functionalized PIM-1, Journal of Membrane Science 457 (2014) 95–102. https://doi.org/10.1016/j.memsci.2014.01.055.
- [15] K. Mizrahi Rodriguez, A.X. Wu, Q. Qian, G. Han, S. Lin, F.M. Benedetti, H. Lee, W.S. Chi, C.M. Doherty, Z.P. Smith, Facile and Time-Efficient Carboxylic Acid Functionalization of PIM-1: Effect on Molecular Packing and Gas Separation Performance, Macromolecules 53 (2020) 6220–6234. https://doi.org/10.1021/acs.macromol.0c00933.
- [16] N. Du, G.P. Robertson, J. Song, I. Pinnau, M.D. Guiver, High-Performance Carboxylated Polymers of Intrinsic Microporosity (PIMs) with Tunable Gas Transport Properties, Macromolecules 42 (2009) 6038–6043. https://doi.org/10.1021/ma9009017.
- [17] K. Mizrahi Rodriguez, F.M. Benedetti, N. Roy, A.X. Wu, Z.P. Smith, Sorption-enhanced mixed-gas transport in amine functionalized polymers of intrinsic microporosity (PIMs), J. Mater. Chem. A 9 (2021) 23631–23642. https://doi.org/10.1039/D1TA06530K.
- [18] C.R. Mason, L. Maynard-Atem, K.W.J. Heard, B. Satilmis, P.M. Budd, K. Friess, M. Lanč, P. Bernardo, G. Clarizia, J.C. Jansen, Enhancement of CO2 Affinity in a Polymer of Intrinsic Microporosity by Amine Modification, Macromolecules 47 (2014) 1021–1029. https://doi.org/10.1021/ma401869p.
- [19] B. Satilmis, M. Lanč, A. Fuoco, C. Rizzuto, E. Tocci, P. Bernardo, G. Clarizia, E. Esposito, M. Monteleone, M. Dendisová, K. Friess, P.M. Budd, J.C. Jansen, Temperature and pressure dependence of gas permeation in amine-modified PIM-1, Journal of Membrane Science 555 (2018) 483–496. https://doi.org/10.1016/j.memsci.2018.03.039.
- [20] B. Satilmis, P. M. Budd, Base-catalysed hydrolysis of PIM-1: amide versus carboxylate formation, RSC Advances 4 (2014) 52189–52198. https://doi.org/10.1039/C4RA09907A.
- [21] P. Yanaranop, B. Santoso, R. Etzion, J. Jin, Facile conversion of nitrile to amide on polymers of intrinsic microporosity (PIM-1), Polymer 98 (2016) 244–251. https://doi.org/10.1016/j.polymer.2016.06.041.
- [22] C.R. Mason, L. Maynard-Atem, N.M. Al-Harbi, P.M. Budd, P. Bernardo, F. Bazzarelli, G. Clarizia, J.C. Jansen, Polymer of Intrinsic Microporosity Incorporating Thioamide Functionality: Preparation and Gas Transport Properties, Macromolecules 44 (2011) 6471–6479. https://doi.org/10.1021/ma200918h.
- [23] N. Du, G.P. Robertson, M.M. Dal-Cin, L. Scoles, M.D. Guiver, Polymers of intrinsic microporosity (PIMs) substituted with methyl tetrazole, Polymer 53 (2012) 4367–4372. https://doi.org/10.1016/j.polymer.2012.07.055.
- [24] W.J. Koros, C. Zhang, Materials for next-generation molecularly selective synthetic membranes, Nature Mater 16 (2017) 289–297. https://doi.org/10.1038/nmat4805.
- [25] M.L. Jue, R.P. Lively, PIM hybrids and derivatives: how to make a good thing better, Current Opinion in Chemical Engineering 35 (2022) 100750. https://doi.org/10.1016/j.coche.2021.100750.
- [26] Y.S. Chang, P. Kumari, C.J. Munro, G. Szekely, L.F. Vega, S. Nunes, L.F. Dumée, Plasticization mitigation strategies for gas and liquid filtration membranes A review, Journal of Membrane Science 666 (2023) 121125. https://doi.org/10.1016/j.memsci.2022.121125.
- [27] F. Kadirkhan, P.S. Goh, A.F. Ismail, W.N.F. Wan Mustapa, M.H.M. Halim, W.K. Soh, S.Y. Yeo, Recent Advances of Polymeric Membranes in Tackling Plasticization and Aging for Practical Industrial CO2/CH4 Applications—A Review, Membranes 12 (2022) 71. https://doi.org/10.3390/membranes12010071.

- [28] A.M.W. Hillock, W.J. Koros, Cross-Linkable Polyimide Membrane for Natural Gas Purification and Carbon Dioxide Plasticization Reduction, Macromolecules 40 (2007) 583–587. https://doi.org/10.1021/ma062180o.
- [29] J.D. Wind, C. Staudt-Bickel, D.R. Paul, W.J. Koros, The Effects of Crosslinking Chemistry on CO2 Plasticization of Polyimide Gas Separation Membranes, Ind. Eng. Chem. Res. 41 (2002) 6139–6148. https://doi.org/10.1021/ie0204639.
- [30] J.D. Wind, C. Staudt-Bickel, D.R. Paul, W.J. Koros, Solid-State Covalent Cross-Linking of Polyimide Membranes for Carbon Dioxide Plasticization Reduction, Macromolecules 36 (2003) 1882–1888. https://doi.org/10.1021/ma025938m.
- [31] A.M. Kratochvil, W.J. Koros, Decarboxylation-Induced Cross-Linking of a Polyimide for Enhanced CO2 Plasticization Resistance, Macromolecules 41 (2008) 7920–7927. https://doi.org/10.1021/ma801586f.
- [32] L. Cui, W. Qiu, D.R. Paul, W.J. Koros, Responses of 6FDA-based polyimide thin membranes to CO2 exposure and physical aging as monitored by gas permeability, Polymer 52 (2011) 5528–5537. https://doi.org/10.1016/j.polymer.2011.10.008.
- [33] W. Qiu, C.-C. Chen, L. Xu, L. Cui, D.R. Paul, W.J. Koros, Sub-Tg Cross-Linking of a Polyimide Membrane for Enhanced CO2 Plasticization Resistance for Natural Gas Separation, Macromolecules 44 (2011) 6046–6056. https://doi.org/10.1021/ma201033j.
- [34] N. Du, M.M. Dal-Cin, G.P. Robertson, M.D. Guiver, Decarboxylation-Induced Cross-Linking of Polymers of Intrinsic Microporosity (PIMs) for Membrane Gas Separation, Macromolecules 45 (2012) 5134–5139. https://doi.org/10.1021/ma300751s.
- [35] C. Zhang, Decarboxylation crosslinking of polyimides with high CO2/CH4 separation performance and plasticization resistance, Journal of Membrane Science (2017) 11.
- [36] H.J. Yu, C.-H. Chan, S.Y. Nam, S.-J. Kim, J.S. Yoo, J.S. Lee, Thermally cross-linked ultrarobust membranes for plasticization resistance and permeation enhancement A combined theoretical and experimental study, Journal of Membrane Science 646 (2022) 120250. https://doi.org/10.1016/j.memsci.2021.120250.
- [37] Y. Shi, Z. Wang, Y. Shi, S. Zhu, Y. Zhang, J. Jin, Synergistic Design of Enhanced π–π Interaction and Decarboxylation Cross-Linking of Polyimide Membranes for Natural Gas Separation, Macromolecules 55 (2022) 2970–2982. https://doi.org/10.1021/acs.macromol.1c02573.
- [38] T. Zhang, L. Deng, P. Li, Decarboxylation Cross-Linking of Triptycene-Based Tröger's Base Polymers for Gas Separation, Ind. Eng. Chem. Res. (2020) 9.
- [39] M. Calle, H.J. Jo, C.M. Doherty, A.J. Hill, Y.M. Lee, Cross-Linked Thermally Rearranged Poly(benzoxazole-co-imide) Membranes Prepared from ortho-Hydroxycopolyimides Containing Pendant Carboxyl Groups and Gas Separation Properties, Macromolecules 48 (2015) 2603–2613. https://doi.org/10.1021/acs.macromol.5b00298.
- [40] W.-N. Wu, K. Mizrahi Rodriguez, N. Roy, J.J. Teesdale, G. Han, A. Liu, Z.P. Smith, Engineering the Polymer–MOF Interface in Microporous Composites to Address Complex Mixture Separations, ACS Appl. Mater. Interfaces 15 (2023) 52893–52907. https://doi.org/10.1021/acsami.3c11300.
- [41] N. Tien-Binh, D. Rodrigue, S. Kaliaguine, In-situ cross interface linking of PIM-1 polymer and UiO-66-NH2 for outstanding gas separation and physical aging control, Journal of Membrane Science 548 (2018) 429–438. https://doi.org/10.1016/j.memsci.2017.11.054.
- [42] B. Lopez-Iglesias, F. Suárez-García, C. Aguilar-Lugo, A. González Ortega, C. Bartolomé, J.M. Martínez-Ilarduya, J.G. de la Campa, Á.E. Lozano, C. Álvarez, Microporous Polymer

- Networks for Carbon Capture Applications, ACS Appl. Mater. Interfaces 10 (2018) 26195–26205. https://doi.org/10.1021/acsami.8b05854.
- [43] C. Aguilar-Lugo, F. Suárez-García, A. Hernández, J.A. Miguel, Á.E. Lozano, J.G. de la Campa, C. Álvarez, New Materials for Gas Separation Applications: Mixed Matrix Membranes Made from Linear Polyimides and Porous Polymer Networks Having Lactam Groups, Ind. Eng. Chem. Res. 58 (2019) 9585–9595. https://doi.org/10.1021/acs.iecr.9b01402.
- [44] G. Zhu, F. Zhang, M.P. Rivera, X. Hu, G. Zhang, C.W. Jones, R.P. Lively, Molecularly Mixed Composite Membranes for Advanced Separation Processes, Angewandte Chemie International Edition 58 (2019) 2638–2643. https://doi.org/10.1002/anie.201811341.
- [45] C.H. Lau, P.T. Nguyen, M.R. Hill, A.W. Thornton, K. Konstas, C.M. Doherty, R.J. Mulder, L. Bourgeois, A.C.Y. Liu, D.J. Sprouster, J.P. Sullivan, T.J. Bastow, A.J. Hill, D.L. Gin, R.D. Noble, Ending Aging in Super Glassy Polymer Membranes, Angew. Chem. Int. Ed. 53 (2014) 5322–5326. https://doi.org/10.1002/anie.201402234.
- [46] C.H. Lau, K. Konstas, C.M. Doherty, S. Kanehashi, B. Ozcelik, S.E. Kentish, A.J. Hill, M.R. Hill, Tailoring Physical Aging in Super Glassy Polymers with Functionalized Porous Aromatic Frameworks for CO2 Capture, Chem. Mater. 27 (2015) 4756–4762. https://doi.org/10.1021/acs.chemmater.5b01537.
- [47] W.J. Koros, D.R. Paul, A.A. Rocha, Carbon dioxide sorption and transport in polycarbonate, J. Polym. Sci. Polym. Phys. Ed. 14 (1976) 687–702. https://doi.org/10.1002/pol.1976.180140410.
- [48] W.J. Koros, D.R. Paul, G.S. Huvard, Energetics of gas sorption in glassy polymers, Polymer 20 (1979) 956–960. https://doi.org/10.1016/0032-3861(79)90192-7.
- [49] D.R. Paul, W.J. Koros, Effect of partially immobilizing sorption on permeability and the diffusion time lag, J. Polym. Sci. Polym. Phys. Ed. 14 (1976) 675–685. https://doi.org/10.1002/pol.1976.180140409.
- [50] W.J. Box, Z. Huang, R. Guo, M. Galizia, The mechanism of light gas transport through configurational free volume in glassy polymers, Journal of Membrane Science 656 (2022) 120608. https://doi.org/10.1016/j.memsci.2022.120608.
- [51] W.J. Box, Z. Huang, R. Guo, M. Galizia, Evidence for Size-Sieving Driven Vapor Sorption and Diffusion in a Glassy Polybenzoxazole Exhibiting Configurational Free Volume, Ind. Eng. Chem. Res. 60 (2021) 13326–13337. https://doi.org/10.1021/acs.iecr.1c02660.
- [52] W.J. Box, L.C. Condes, M.T. Webb, A. Suleiman, R. Guo, M. Galizia, Computer vision-based measurement of pure- and mixed-gas swelling in polymer membranes: individual and synergistic effects of configurational free volume and thermal rearrangement, Journal of Membrane Science Under Review (2024).
- [53] A.C. Puleo, D.R. Paul, S.S. Kelley, The effect of degree of acetylation on gas sorption and transport behavior in cellulose acetate, Journal of Membrane Science 47 (1989) 301–332. https://doi.org/10.1016/S0376-7388(00)83083-5.
- [54] W.J. Box, M.T. Webb, M. Galizia, Evaluating the Experimental Uncertainty in Gas and Vapor Sorption/Adsorption Measurements: Fundamental Considerations and Experimental Design Implications, Ind. Eng. Chem. Res. 61 (2022) 9856–9868. https://doi.org/10.1021/acs.iecr.2c01414.
- [55] M. Galizia, Z.P. Smith, G.C. Sarti, B.D. Freeman, D.R. Paul, Predictive calculation of hydrogen and helium solubility in glassy and rubbery polymers, Journal of Membrane Science 475 (2015) 110–121. https://doi.org/10.1016/j.memsci.2014.10.009.

- [56] M. Mahato, R. Tabassian, V.H. Nguyen, S. Oh, S. Nam, W.-J. Hwang, I.-K. Oh, CTF-based soft touch actuator for playing electronic piano, Nat Commun 11 (2020) 5358. https://doi.org/10.1038/s41467-020-19180-3.
- [57] L. Hao, K.-S. Liao, T.-S. Chung, Photo-oxidative PIM-1 based mixed matrix membranes with superior gas separation performance, J. Mater. Chem. A 3 (2015) 17273–17281. https://doi.org/10.1039/C5TA03776J.
- [58] P. Wang, X. Li, Z. Liu, J. Peng, C. Shi, T. Li, J. Yang, C. Shan, W. Hu, B. Liu, Construction of highly conductive PBI-based alloy membranes by incorporating PIMs with optimized molecular weights for high-temperature proton exchange membrane fuel cells, Journal of Membrane Science 659 (2022) 120790. https://doi.org/10.1016/j.memsci.2022.120790.
- [59] P.F. Muldoon, S.R. Venna, D.W. Gidley, J.S. Baker, L. Zhu, Z. Tong, F. Xiang, D.P. Hopkinson, S. Yi, A.K. Sekizkardes, N.L. Rosi, Mixed Matrix Membranes from a Microporous Polymer Blend and Nanosized Metal-Organic Frameworks with Exceptional CO2/N2 Separation Performance, ACS Materials Lett. 2 (2020) 821–828. https://doi.org/10.1021/acsmaterialslett.0c00156.
- [60] A.Yu. Alentiev, G.N. Bondarenko, Yu.V. Kostina, V.P. Shantarovich, S.N. Klyamkin, V.P. Fedin, K.A. Kovalenko, Yu.P. Yampolskii, PIM-1/MIL-101 hybrid composite membrane material: Transport properties and free volume, Pet. Chem. 54 (2014) 477–481. https://doi.org/10.1134/S0965544114070020.
- [61] M. Yahia, Q.N. Phan Le, N. Ismail, M. Essalhi, O. Sundman, A. Rahimpour, M.M. Dal-Cin, N. Tavajohi, Effect of incorporating different ZIF-8 crystal sizes in the polymer of intrinsic microporosity, PIM-1, for CO2/CH4 separation, Microporous and Mesoporous Materials 312 (2021) 110761. https://doi.org/10.1016/j.micromeso.2020.110761.
- [62] M. Yu, A.B. Foster, M. Alshurafa, J.M. Luque-Alled, P. Gorgojo, S.E. Kentish, C.A. Scholes, P.M. Budd, CO2 separation using thin film composite membranes of acid-hydrolyzed PIM-1, Journal of Membrane Science 679 (2023) 121697. https://doi.org/10.1016/j.memsci.2023.121697.
- [63] B. Santoso, P. Yanaranop, H. Kang, I.K.H. Leung, J. Jin, A Critical Update on the Synthesis of Carboxylated Polymers of Intrinsic Microporosity (C-PIMs), Macromolecules 50 (2017) 3043–3050. https://doi.org/10.1021/acs.macromol.7b00344.
- [64] J.P. Kokko, Leon. Mandell, J.H. Goldstein, An N.m.r. Investigation of Proton Mobility in Substituted Uracils, J. Am. Chem. Soc. 84 (1962) 1042–1047. https://doi.org/10.1021/ja00865a035.
- [65] T.P. Eskay, P.F. Britt, A.C.B. Iii, Pyrolysis of Aromatic Carboxylic Acids: Potential Involvement of Anhydrides in Retrograde Reactions in Low-Rank Coal, Energy Fuels 11 (1997) 1278–1287.
- [66] F.Y. Li, Y. Xiao, T.-S. Chung, S. Kawi, High-Performance Thermally Self-Cross-Linked Polymer of Intrinsic Microporosity (PIM-1) Membranes for Energy Development, Macromolecules 45 (2012) 1427–1437. https://doi.org/10.1021/ma202667y.
- [67] L. Wang, X. Guo, F. Zhang, N. Li, Blending and *in situ* thermally crosslinking of dual rigid polymers for anti-plasticized gas separation membranes, Journal of Membrane Science 638 (2021) 119668. https://doi.org/10.1016/j.memsci.2021.119668.
- [68] T.K. Eriksen, B.K.V. Hansen, J. Spanget-Larsen, The Vibrational Structure of Dibenzo-p-dioxin. IR Linear Dichroism, Raman Spectroscopy, and Quantum Chemical Calculations, Polish Journal of Chemistry 82 (2008) 921–934.

- [69] W. Chen, Z. Zhang, L. Hou, C. Yang, H. Shen, K. Yang, Z. Wang, Metal-organic framework MOF-801/PIM-1 mixed-matrix membranes for enhanced CO2/N2 separation performance, Separation and Purification Technology 250 (2020) 117198. https://doi.org/10.1016/j.seppur.2020.117198.
- [70] L. Hou, Z. Wang, Z. Chen, W. Chen, C. Yang, PIM-1 as an organic filler to enhance CO2 separation performance of poly (arylene fluorene ether ketone), Separation and Purification Technology 242 (2020) 116766. https://doi.org/10.1016/j.seppur.2020.116766.
- [71] O.A. Mkhatresh, F. Heatley, Thermal oxidative and photo-oxidative degradation of polytetrahydrofuran studied using 1H NMR, 13C NMR and GPC, Polymer International 53 (2004) 959–971. https://doi.org/10.1002/pi.1483.
- [72] K. Matsuda, Y. Tanaka, T. Sakai, Effect of perchloric acid on the molecular weight and yield of poly-THF, J of Applied Polymer Sci 20 (1976) 2821–2827. https://doi.org/10.1002/app.1976.070201016.
- [73] T.C. Chang, K.H. Wu, H.B. Chen, S.Y. Ho, Y.S. Chiu, Thermal degradation of aged polytetrahydrofuran and its copolymers with 3-azidomethyl-3'-methyloxetane and 3-nitratomethyl-3'-methyloxetane by thermogravimetry, Journal of Polymer Science Part A: Polymer Chemistry 34 (1996) 3337–3343. https://doi.org/10.1002/(SICI)1099-0518(19961130)34:16<3337::AID-POLA10>3.0.CO;2-H.
- [74] W.E. Wallace, Mass Spectra, in: NIST Chemistry WebBook, NIST Standard Reference Database Number 69, National Institute of Standards and Technology, Gaithersburg MD, 20899, n.d. https://webbook.nist.gov/cgi/cbook.cgi?ID=C109999&Units=SI&Mask=200#Mass-Spec (accessed November 17, 2023).
- [75] K. Tago, M. Tsuchiya, Y. Gondo, K. Ishimaru, T. Kojima, Thermal decomposition of poly(oxytetramethylene) glycol, Journal of Applied Polymer Science 77 (2000) 1538–1544. https://doi.org/10.1002/1097-4628(20000815)77:7<1538::AID-APP15>3.0.CO;2-J.
- [76] K. Ghosal, R.T. Chern, B.D. Freeman, W.H. Daly, I.I. Negulescu, Effect of Basic Substituents on Gas Sorption and Permeation in Polysulfone, Macromolecules 29 (1996) 4360–4369. https://doi.org/10.1021/ma951310i.
- [77] H.W. Kim, H.B. Park, Gas diffusivity, solubility and permeability in polysulfone–poly(ethylene oxide) random copolymer membranes, Journal of Membrane Science 372 (2011) 116–124. https://doi.org/10.1016/j.memsci.2011.01.053.
- [78] S.M. Jordan, W.J. Koros, G.K. Fleming, The effects of CO2 exposure on pure and mixed gas permeation behavior: comparison of glassy polycarbonate and silicone rubber, Journal of Membrane Science 30 (1987) 191–212. https://doi.org/10.1016/S0376-7388(00)81351-4.
- [79] T.-S. Chung, S.S. Chan, R. Wang, Z. Lu, C. He, Characterization of permeability and sorption in Matrimid/C60 mixed matrix membranes, Journal of Membrane Science 211 (2003) 91–99. https://doi.org/10.1016/S0376-7388(02)00385-X.
- [80] E. Esposito, I. Mazzei, M. Monteleone, A. Fuoco, M. Carta, N.B. McKeown, R. Malpass-Evans, J.C. Jansen, Highly Permeable Matrimid®/PIM-EA(H2)-TB Blend Membrane for Gas Separation, Polymers 11 (2019) 46. https://doi.org/10.3390/polym11010046.
- [81] M.T. Webb, L.C. Condes, H.G. Ly, M. Galizia, S. Razavi, Rational design, synthesis, and characterization of facilitated transport membranes exhibiting enhanced permeability, selectivity and stability, Journal of Membrane Science 685 (2023) 121910. https://doi.org/10.1016/j.memsci.2023.121910.

- [82] Y. Kinoshita, K. Wakimoto, A.H. Gibbons, A.P. Isfahani, H. Kusuda, E. Sivaniah, B. Ghalei, Enhanced PIM-1 membrane gas separation selectivity through efficient dispersion of functionalized POSS fillers, Journal of Membrane Science 539 (2017) 178–186. https://doi.org/10.1016/j.memsci.2017.05.072.
- [83] A.F. Bushell, P.M. Budd, M.P. Attfield, J.T.A. Jones, T. Hasell, A.I. Cooper, P. Bernardo, F. Bazzarelli, G. Clarizia, J.C. Jansen, Nanoporous Organic Polymer/Cage Composite Membranes, Angewandte Chemie International Edition 52 (2013) 1253–1256. https://doi.org/10.1002/anie.201206339.
- [84] X. Wu, Z. Tian, S. Wang, D. Peng, L. Yang, Y. Wu, Q. Xin, H. Wu, Z. Jiang, Mixed matrix membranes comprising polymers of intrinsic microporosity and covalent organic framework for gas separation, Journal of Membrane Science 528 (2017) 273–283. https://doi.org/10.1016/j.memsci.2017.01.042.
- [85] R. Hou, S.J.D. Smith, C.D. Wood, R.J. Mulder, C.H. Lau, H. Wang, M.R. Hill, Solvation Effects on the Permeation and Aging Performance of PIM-1-Based MMMs for Gas Separation, ACS Appl. Mater. Interfaces 11 (2019) 6502–6511. https://doi.org/10.1021/acsami.8b19207.
- [86] W. Han, C. Zhang, M. Zhao, F. Yang, Y. Yang, Y. Weng, Post-modification of PIM-1 and simultaneously in situ synthesis of porous polymer networks into PIM-1 matrix to enhance CO2 separation performance, Journal of Membrane Science 636 (2021) 119544. https://doi.org/10.1016/j.memsci.2021.119544.
- [87] Z.P. Smith, D.F. Sanders, C.P. Ribeiro, R. Guo, B.D. Freeman, D.R. Paul, J.E. McGrath, S. Swinnea, Gas sorption and characterization of thermally rearranged polyimides based on 3,3′-dihydroxy-4,4′-diamino-biphenyl (HAB) and 2,2′-bis-(3,4-dicarboxyphenyl) hexafluoropropane dianhydride (6FDA), Journal of Membrane Science 415–416 (2012) 558–567. https://doi.org/10.1016/j.memsci.2012.05.050.
- [88] L. Matesanz-Niño, M.T. Webb, A. González-Ortega, L. Palacio, C. Álvarez, Á.E. Lozano, M. Galizia, Plasticization resistant gas separation membranes derived from polyimides exhibiting polyethylene-oxide moieties, Polymer 290 (2024) 126535. https://doi.org/10.1016/j.polymer.2023.126535.
- [89] W.S. Chi, B.J. Sundell, K. Zhang, D.J. Harrigan, S.C. Hayden, Z.P. Smith, Mixed-Matrix Membranes Formed from Multi-Dimensional Metal—Organic Frameworks for Enhanced Gas Transport and Plasticization Resistance, ChemSusChem 12 (2019) 2355–2360. https://doi.org/10.1002/cssc.201900623.
- [90] Y. He, F.M. Benedetti, S. Lin, C. Liu, Y. Zhao, H.-Z. Ye, T. Van Voorhis, M.G. De Angelis, T.M. Swager, Z.P. Smith, Polymers with Side Chain Porosity for Ultrapermeable and Plasticization Resistant Materials for Gas Separations, Advanced Materials 31 (2019) 1807871. https://doi.org/10.1002/adma.201807871.
- [91] X. Jiang, S. Li, S. He, Y. Bai, L. Shao, Interface manipulation of CO 2 –philic composite membranes containing designed UiO-66 derivatives towards highly efficient CO 2 capture, Journal of Materials Chemistry A 6 (2018) 15064–15073. https://doi.org/10.1039/C8TA03872D.
- [92] H. Yin, Y.Z. Chua, B. Yang, C. Schick, W.J. Harrison, P.M. Budd, M. Böhning, A. Schönhals, First Clear-Cut Experimental Evidence of a Glass Transition in a Polymer with Intrinsic Microporosity: PIM-1, J. Phys. Chem. Lett. 9 (2018) 2003–2008. https://doi.org/10.1021/acs.jpclett.8b00422.

- [93] P.R. Bevington, D.K. Robinson, Data reduction and error analysis for the physical sciences, 3rd ed, McGraw-Hill, Boston, 2003.
- [94] A. Bos, I.G.M. Pünt, M. Wessling, H. Strathmann, CO2-induced plasticization phenomena in glassy polymers, Journal of Membrane Science 155 (1999) 67–78. https://doi.org/10.1016/S0376-7388(98)00299-3.